# Synapse-specific Opioid Modulation of Thalamo-cortico-striatal Circuits

William T. Birdsong[1,4,*], Bart C. Jongbloets[1,*], Kim A. Engeln[1], Dong Wang[2], Gregory Scherrer[2,3], and Tianyi Mao[1]

*1. Vollum Institute, Oregon Health & Science University, Portland, OR 97239, USA*

*2. Department of Anesthesiology, Perioperative and Pain Medicine, Department of Molecular and Cellular Physiology, Department of Neurosurgery, Stanford Neurosciences Institute, Stanford University, Palo Alto, CA 94305, USA*

*3. New York Stem Cell Foundation – Robertson Investigator, Stanford University, Palo Alto, CA 94304, USA*

*4. Current address: Department of Pharmacology, University of Michigan, Ann Arbor, MI 48109, USA*

*: These authors contributed equally.

Correspondence should be addressed to W.T.B. (wtbird@med.umich.edu) or T.M. (mao@ohsu.edu).

Lead Contact: Dr. Tianyi Mao

Vollum Institute, Oregon Health & Science University

3181 SW Sam Jackson Park Road, L474

Portland, Oregon 97239, USA

(503) 494-9286 / mao@ohsu.edu

## Abstract

The medial thalamus (MThal), anterior cingulate cortex (ACC) and striatum play important roles in affective-motivational pain processing and reward learning. Opioids affect both pain and reward through uncharacterized modulation of this circuitry. This study examined opioid actions on glutamate transmission between these brain regions in mouse. Mu-opioid receptor (MOR) agonists potently inhibited MThal inputs without affecting ACC inputs to individual striatal medium spiny neurons (MSNs). MOR activation also inhibited MThal inputs to the pyramidal neurons in the ACC. In contrast, delta-opioid receptor (DOR) agonists disinhibited ACC pyramidal neuron responses to MThal inputs by suppressing local feed-forward GABA signaling from parvalbumin-positive interneurons. As a result, DOR activation in the ACC facilitated poly-synaptic (thalamo-cortico-striatal) excitation of MSNs by MThal inputs. These results suggest that opioid effects on pain and reward may be shaped by the relative selectivity of opioid drugs to the specific circuit components.


Keywords: Opioids, thalamus, striatum, anterior cingulate cortex, affective pain, mu opioid receptor, delta opioid receptor, feed-forward inhibition

## Introduction

Opioids blunt both sensory-discriminative and affective-motivational dimensions of pain by modulating neuronal activity in the central and peripheral nervous systems (Oertel et al., 2008; Zubieta et al. 2001, Corder et al. 2018). The affective-motivational dimension of pain underlies the aversiveness and negative emotional affect that arise in response to activation of nociceptive inputs (Gracely 1992; Navratilova & Porreca, 2014; Treede et al., 1999). This study examines how opioids modulate the circuitry involved in affective-motivational pain perception.

In humans, affective pain perception is associated with increased activity in the medial thalamus, as well as the anterior cingulate cortex (ACC) (Casey et al., 1994; Davis et al., 1997; Peyron et al., 1999, Peyron et al., 2000). In rodents, chronic pain is associated with hypersensitivity of mediodorsal thalamic neurons to sensory stimuli (Whitt et al., 2013) and activation of the ACC has been shown to be aversive using a conditioned place aversion paradigm (Johansen and Fields, 2004). In contrast, lesions of the ACC decrease affective-motivational pain responses (Johansen et al., 2001). Anatomically, neurons from the medial thalamus (MThal) send glutamate afferents to the cortical regions, including the dorsal and ventral ACC, prefrontal cortex (PFC) and insular cortices (Hunnicutt at al., 2014), as well as to the dorsomedial striatum (DMS) (Hunnicutt at al., 2016). The ACC in turn projects to the DMS, forming a circuit connecting the medial thalamus and the ACC, both of which provide convergent glutamate inputs to the DMS. This thalamo-cortico-striatal circuit has been demonstrated to be involved in pain processing, in particular, affective pain perception (Rainville et al., 1997; Price, 2000, Fields, 2004; Zhang et al., 2015; Yokota et al., 2016).

Clinically, opioids are used to reduce pain perception by modulating both sensory-discriminative and affective-motivational aspects of pain. Mu-opioid receptors (MORs) and delta-opioid receptors (DORs) are predominantly expressed in the mediodorsal (MD) thalamus and ACC, respectively (Mansour et al, 1994; Erbs et al. 2015). Injection of opioids into the MD or ACC can relieve pain and induce conditioned place preference in an animal model of chronic pain (Carr and Bak, 1988; Guo et al., 2008; Navritalova et al., 2015), suggesting a role for opioid modulation of thalamic and cortical circuitry in affective pain.

The striatum is enriched in MORs and DORs, as well as the endogenous opioid ligand enkephalin (Pert et al., 1976, Koshimizu et al., 2008). Also, opioids have been shown to inhibit glutamate inputs to the striatum, as well as GABA release from local striatal circuitry (Jiang and North, 1992; Hoffman and Lupica, 2001; Brundege and Williams, 2002; Miura et al., 2007; Atwood et al., 2014; Banghart et al., 2015). In this context, the striatum serves as a potentially critical hub for opioid-dependent modulation of fast synaptic transmission in the affective pain circuitry (Zubieta et al. 2001).

The current work determines how and where opioids modulate synaptic transmission between the thalamic, cortical and striatal regions that are important for the perception of affective pain. Results revealed opposing roles of the MORs and DORs regarding information flow from the thalamus to the striatum, whereby MOR activation decreased glutamate transmission in the striatum, while DOR activation facilitated glutamate transmission via disinhibition of cortical pyramidal neurons. Thus, MOR activation is predicted to blunt affective pain, while DOR activation is predicted to facilitate affective pain perception. Together, these data identify

specific synaptic connections within the thalamo-cortico-striatal circuit that are modulated by opioids and illustrate how different opioid subtypes can independently modulate neuronal communication at the circuit level.

## Results

### Opioid receptor agonists suppress excitatory transmission in the dorsomedial striatum

Because the DMS mediates learning and expression of motivated behaviors in response to both aversive and rewarding stimuli, the opioid sensitivity of glutamate afferents in the DMS was investigated. In acute mouse brain slice preparations, individual striatal medium spiny neurons (MSNs) were identified based on physiological properties (Kreitzer, 2009). Whole-cell voltage-clamp recordings were obtained and glutamate release was evoked using electrical stimulation. AMPA receptor mediated excitatory postsynaptic currents (EPSCs) were pharmacologically isolated and recorded (**Figure 1 – figure supplement 1a-c**). Similar to previously published results in the nucleus accumbens and dorsolateral striatum, application of the mu- and delta-selective opioid agonist [Met$^5$]-enkephalin (ME, 3 µM) significantly decreased the amplitude of the EPSCs. This inhibition was reversed upon washout of ME (**Figure 1 – figure supplement 1c**; ME: 77.8 ± 4.6% of baseline; washout: 90.5 ± 2.6% of baseline; baseline vs ME: $W(11) = 1$, $p < 0.01$) (Jiang and North, 1992; Hoffman and Lupica, 2001; Brundege and Williams, 2002). The AMPA receptor antagonist NBQX (3 µM) eliminated the evoked currents (**Figure 1 – figure supplement 1c**, 4.0 ± 2.6% of baseline; baseline vs NBQX: $W(5) = 0$, $p < 0.05$).

### Mu-opioid receptor agonists suppress thalamic but not cortical glutamatergic inputs to the dorsomedial striatum

Anatomic mapping in mice indicated that glutamate inputs from the medial thalamus and ACC converged in the DMS **(Figure 1a-b** and **figure 1 – figure supplement 1d-e)** (Hunnicutt et al., 2016). In addition, MORs and DORs appear to be enriched in the medial thalamus and midline cortical structures (including the ACC) respectively (Erbs et al. 2015, Wang et al. 2018). To test whether anatomically distinct expression of MORs and DORs in the thalamus and the cortex confer specific opioid sensitivity to these two inputs to the striatum, an optogenetic approach was used to isolate the specific thalamic and cortical inputs onto MSNs in the DMS. Recombinant adeno-associated viruses (AAVs) encoding two optically-separable channelrhodopsin variants were injected into the MThal and ACC of three- to five-week-old mice (**Figure 1a**). The blue light-sensitive channelrhodopsins (CsChR or ChR2(H134R)) were expressed in the MThal while the red light-sensitive channelrhodopsin (Chrimson) was expressed in the ACC (Klapoetke et al., 2014). Expression of one channelrhodopsin variant alone demonstrated wavelength-selectivity of optically-evoked excitatory postsynaptic currents (oEPSCs) in response to brief pulses of either blue (470 nm) or red (625 nm) light, and minimal cross contamination from undesired light stimulation was observed under these conditions (**Figure 1 – figure supplement 1d-e**). Following co-expression of Chrimson in the ACC and either CsChR or ChR2(H134R) in the MThal, illumination with both blue (470 nm, MThal inputs) and red light (625 nm, ACC inputs) evoked robust oEPSCs in individual MSNs in the DMS (**Figure 1b**). The MOR-selective agonist DAMGO inhibited oEPSC amplitude to MThal stimulation (470 nm light) in a reversible manner, and did not alter oEPSC amplitude to ACC stimulation (**Figure 1c**; DAMGO $I_{MThal}$: 38.2 ± 6.1% of baseline, $z = 4.738$, $p < 0.001$; $I_{ACC}$: 92.8 ± 4.9 %, $z = 0.459$, $p = 0.647$). These observations demonstrated both the optical separation of the thalamic and cortical inputs and the ability of MOR agonists to selectively inhibit excitatory MThal inputs. Despite the apparent

expression of DORs in the midline cortical regions, DOR activation by its selective agonist DPDPE did not inhibit the ACC, or MThal inputs (**Figure 1b-d**; DPDPE $I_{MThal}$: 99.6 ± 5.7 % of baseline, $z = 0.106$, $p = 0.916$; $I_{ACC}$: 95.6 ± 2.6 %, $z = 0.196$, $p = 0.845$).

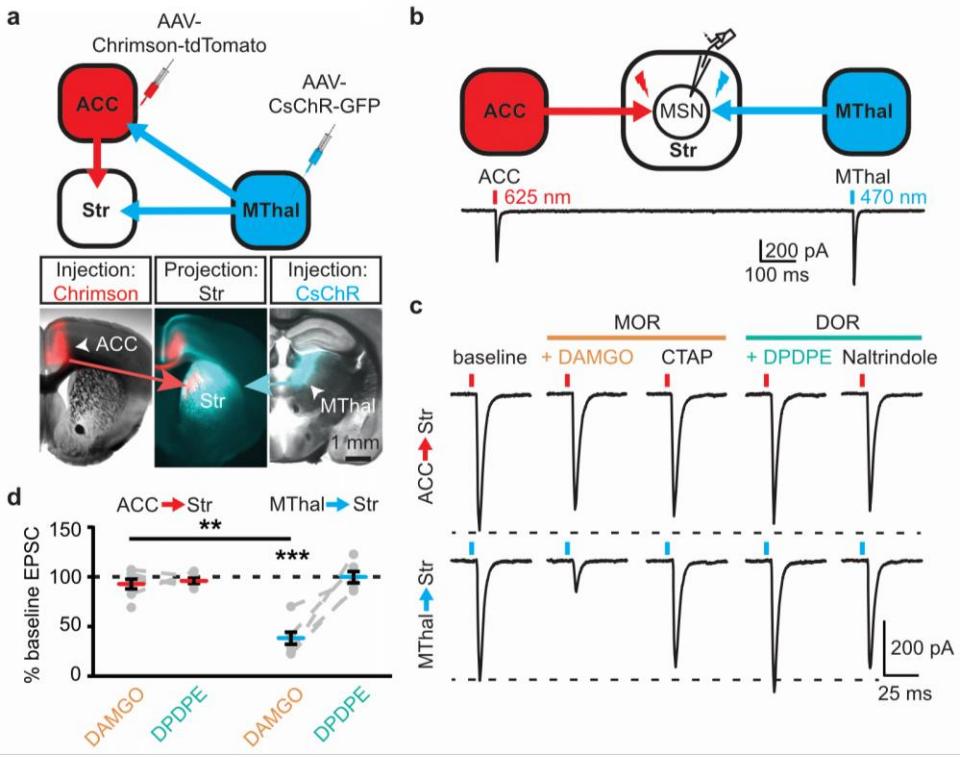


**Figure 1. Mu-opioid agonists suppress thalamic but not cortical inputs to single MSNs in the striatum**

(**a**) Schematic (upper panel) and an acute mouse brain slice example (lower panel) of viral injection design and the axonal projections to the striatum. Overlaid brightfield and epifluorescent images showing the injection site of Chrimson (left image, red) in the ACC, and CsChR (right image, cyan) in the MThal, and convergent axonal projections from both injections to the DMS (center image). (**b**) Schematic (upper panel) and representative recordings (lower panel) for optical excitation. (**c**) Example oEPSCs of individual MSNs evoked by 625 nm (from the ACC, upper traces), and by 470 nm (from the MThal, lower traces) light pulses. The MOR (orange label) agonist DAMGO (1 µM) was perfused followed by the MOR antagonist CTAP (1

144 µM). Following CTAP, the DOR (teal label) agonist DPDPE (1 µM) was perfused followed by
145 the moderately-selective DOR antagonist naltrindole (0.3 µM). Red bars: 3 ms of 625 nm light
146 stimulation; blue bars: 1 ms of 470 nm light stimulation. (**d**) Summary data of dual wavelength
147 excitation of the ACC and MThal input oEPSCs recorded from single MSNs. Data are plotted as
148 the percentage of baseline current following exposure to DAMGO or DPDPE for inputs from the
149 ACC and MThal (N = 5, n = 8, Linear mixed model: 3-way interaction, opioid type (mu vs. delta
150 opioid) x input source (ACC vs. MThal) x drug condition (baseline vs. agonist vs. antagonist), $F(4,8) = 2.938$, $p = 0.091$; $MThal_{baseline\ x\ DAMGO}$: $z = 4.738$, $p < 0.001$; $MThal_{baseline\ x\ DAMGO}$ vs.
152 $ACC_{baseline\ x\ DAMGO}$; $z = -3.026$, $p < 0.01$). Mean ± standard error of the mean. Str: striatum.
153 The following figure supplement is available for figure 1:
154 **Figure supplement 1**. Mu-opioid agonists suppress thalamic, but not cortical inputs.
155 **Figure supplement 2**. Single channelrhodopsin injections reproduced specific effect of mu-
156 opioid-mediated inhibition of thalamic but not cortical inputs.
157
158 Similar results were obtained when Chrimson and CsChR were injected into the MThal and the
159 PFC, respectively (**Figure 1 – figure supplement 1f-g**). DAMGO decreased oEPSC amplitude
160 from the MThal inputs while it had no effect on oEPSCs from the PFC inputs (**Figure 1 – figure**
161 **supplement 1h-i** ; DAMGO $I_{MThal}$: 22.2 ± 3.7 % of baseline, $z = 3.497$, $p < 0.001$; $I_{PFC}$: 93.9 ±
162 5.6 %, $z = 0.052$, $p = 0.958$). DPDPE produced no significant changes in oEPSC amplitude from
163 either input (DPDPE $I_{MThal}$: 96.5 ± 3.9 % of baseline, $z = 0.087$, $p = 0.931$; $I_{PFC}$: 81.6 ± 3.9 %, $z =$
164 0.672, $p = 0.502$). These results indicate that MThal glutamate inputs onto MSNs were
165 preferentially inhibited by activation of MORs, while DOR agonists had little to no modulatory
166 effect on the MThal, ACC, or PFC inputs to the MSNs in the DMS. These findings of mu- and

delta-opioid specificity were further confirmed with similar experiments using single channelrhodopsin variant viral injections into the ACC, PFC, or MThal (**Figure 1 – figure supplement 2**).

To ensure that these opioid-sensitive inputs indeed originated from the MThal, *vGluT2-cre* mice (Vong et al., 2011) were injected with DIO-ChR2(H134R) virus which restricted the expression of ChR2 only to the thalamus (Wu et al., 2015). Similar to the results from wild-type mice, activation of MORs by DAMGO, but not DORs by DPDPE, resulted in inhibition of the MThal inputs to the MSNs (Figure 2; $I_{DAMGO}$: 18.1 ± 3.9 % of baseline, W (6) = 0, $p < 0.05$; $I_{DPDPE}$: 100.5 ± 7.9 %, W (5) = 7, p = 1). Furthermore, MOR agonists also inhibited inputs from the anterior medial thalamus, suggesting the general effects of opioid inhibition of thalamic inputs to the DSM (**Figure 1 – figure supplement 2**).

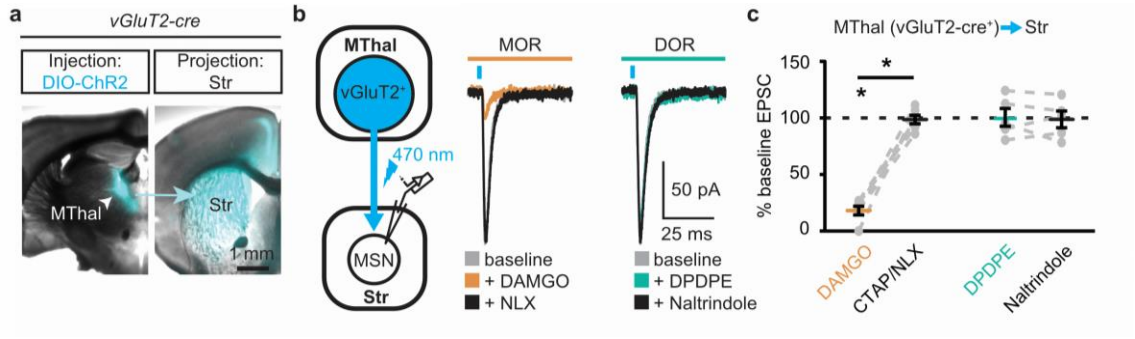


**Figure 2. Mu-opioid agonists selectively suppress thalamic inputs from vGluT2-positive thalamic neurons**

(**a**) Example overlaid brightfield and epifluorescent images showing Cre-dependent expression of ChR2(H134R)-EYFP (cyan) in the MThal (left panel) and axonal projections into the DMS (right panel) following injection of AAV2-DIO-ChR2(H134R)-EYFP in the MThal of *vGluT2-Cre* mice. (**b**) Experimental schematic showing optical stimulation of glutamate inputs in the

DMS (left panel). Representative traces of oEPSCs showing effects of MOR agonist DAMGO (1 µM, middle panel, orange) and antagonist naloxone (NLX, 1 µM, middle panel, black), and the DOR agonist DPDPE (1 µM, right panel, teal) and DOR antagonist naltrindole (0.3 µM, right panel, black). (**c**) Summary data of oEPSCs showing effects of MOR agonist DAMGO and antagonist CTAP or NLX (1 µM), and the DOR agonist DPDPE and DOR antagonist naltrindole. DAMGO/(CTAP/NLX): N = 3, n = 6, *SM* = 9.33, $p < 0.01$; DPDPE/naltrindole, N = 3, n = 5, *SM* = 0, p = 1.0. Skillings-Mack test followed by paired Wilcoxon signed-ranks test *post-hoc* analysis. Mean ± standard error of the mean. * $p \leq 0.05$; *SM*: Skillings-Mack statistic; Str: striatum.

**Thalamostriatal and thalamocortical projections can arise from the same medial thalamic neuronal population**

Single neuron tracing in the rat has demonstrated that medial thalamic neurons can send collaterals to both the cortex and striatum (Otake and Nakamura, 1998; Kuramoto et al., 2017). To determine whether the opioid-sensitive population of thalamic neurons in mouse project to both the ACC and DMS, two approaches were used. First, red and green fluorescent retrograde transported beads (retrobeads) were injected into the ACC and DMS, respectively (**Figure 3 – figure supplement 1b**). The injection sites were then localized based on the mouse brain atlas (Franklin & Paxinos, 2001, **Figure 3 – figure supplement 1b-c**). Retrogradely labeled somas were found in the lateral MD and the central lateral (CL) thalamus (**Figure 3 – figure supplement 1c-g**). In brain sections containing the MD thalamus (selected figures 44, 45, and 46 of the Franklin & Paxinos atlas, second edition; **Figure 3 – figure supplement 1d**), there was a substantial fraction of neurons that projected to the DMS that also contained retrograde beads

originating from the ACC (21 ± 4% of striatal-projecting neurons colocalized with ACC-projecting neurons). Second, to further determine whether cortical-projecting thalamic neurons send collateral axons to the striatum, a retrogradely transported virus, AAV2-retro (Tervo et al., 2016), encoding Cre-recombinase was injected into the ACC, along with AAV2-GFP which served to indicate the injection site of AAV2-retro-Cre virus and to visualize corticostriatal axons (Madisen et al., 2015, Tervo et al., 2016). In the same mice, Cre-dependent AAV2-FLEX-TdTomato virus was injected into the MThal (**Figure 3a-d**). TdTomato would be expected to be expressed only in the thalamic neurons projecting to the ACC area that were also infected by AAV2-retro-Cre virus. Indeed, TdTomato-positive neurons were found in the MThal (**Figure 3b**). GFP expression in the ACC indicated the AAV2-retro virus injection site (**Figure 3c**), and TdTomato-expressing axon terminals, originating from thalamic neurons, were also visible in the ACC (**Figure 3c**). Prominent GFP-expressing axons originating from the ACC and TdTomato-expressing axon collaterals originating from the MThal were observed in the DMS (**Figure 3d**). These results indicate that at least a significant fraction of thalamic neurons project to both the ACC and DMS, and further, ACC-striatal and MThal-striatal projections can innervate anatomically overlapping areas in the DMS (Hunnicutt et al. 2016).

To confirm that the apparent axon collaterals in the DMS form functional synapses rather than passing through the DMS en route to the ACC, AAV2-retro-Cre was injected into the ACC and a Cre-dependent ChR2-expressing virus AAV2-DIO-ChR2(H134R)-EYFP was injected into the MThal, conferring the ability to optogenetically activate potential striatal axons originating from ACC-projecting MThal neurons (**Figure 3e**). Optical illumination evoked glutamate-mediated oEPSCs in striatal MSNs that were potently inhibited by ME (**Figure 3f**; $I_{ME}$: 22.4 ± 6.6% of

baseline, N = 3, n = 5, paired t-test, $p < 0.01$). Thus, a portion of the opioid-sensitive thalamic neuronal population projected to both the DMS and ACC.

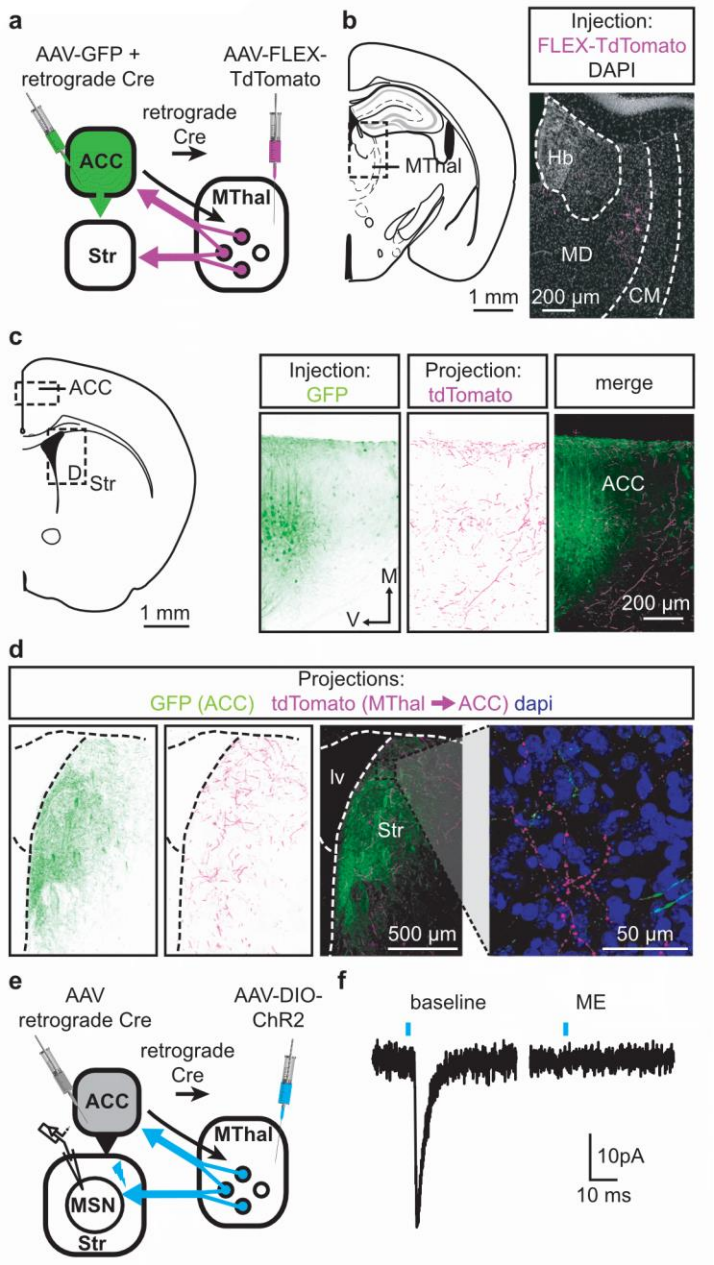


**Figure 3. Individual mediodorsal thalamic neurons project to both the DMS and ACC**

(**a**) Schematic of the AAVretro-Cre and Cre-dependent AAV2-DIO-TdTomato injections. (**b**) Fluorescent image of cell bodies expressing TdTomato following injections shown in (**a**) in the MThal (magenta, right panel), with corresponding mouse brain atlas section (left panel). (**c**)

Representative mouse brain atlas section showing approximate origin of images taken from ACC (left panels) and DMS as shown in (**d**). Images of the ACC showing AAV-GFP injection site and axons from the MThal (magenta). (**d**) Images of the DMS showing overlapping axons from both the ACC (green) and MThal (magenta). Rightmost panel shows high magnification image taken at the black box demarcation in the left panel. Cell nuclei are stained with DAPI (blue). (**e**) Schematic of retrograde AAV-retro-Cre and Cre-dependent AAV2-DIO-ChR2(H134R)-EYFP injections, and recordings of MSNs in the DMS. (**f**) An example trace of oEPSCs of a MSN in the DMS from a mouse injected as shown in (**e**). ME: opioid agonist [Met$^5$]-Enkephalin. Blue bars: 470 nm light stimulation. V: ventral; M: midline; Hb: habenula; CM: centromedial thalamus; MD: mediodorsal thalamus; Str: striatum; lv: lateral ventricle. Mouse brain atlas sections from Franklin & Paxinos 2001.

The following figure supplement is available for figure 3:

**Figure supplement 1**. A subset of mediodorsal thalamic neurons send collaterals to both the ACC and DMS.

## Mu-opioid agonists suppress excitatory thalamic inputs to the ACC, while delta-opioid agonists suppress feedforward inhibition

Since the excitatory MThal inputs to the DMS were strongly inhibited by MOR activation and at least a fraction of those thalamic neurons project to both the ACC and DMS, we hypothesized that the excitatory MThal inputs to the ACC would be inhibited by MORs. Inputs from the MD thalamus have been reported to synapse directly onto layer 2/3 (L2/3) and 5 (L5) pyramidal neurons, and also to trigger GABA release onto pyramidal neurons via innervation of L2/3 and L5 parvalbumin-positive (PV) interneurons in the ACC (Delevich et al., 2015). Both optically

evoked oEPSCs and feed-forward inhibitory postsynaptic currents (oIPSCs) were measured in L2/3 and L5 pyramidal neurons of the ACC (**Figure 4** and **figure 4 – figure supplement 1**; also see **Materials and Methods**). Similar to the results from recordings of the MSNs in the DMS, oEPSCs of the L2/3 and L5 pyramidal neurons in the ACC from the MThal inputs were potently inhibited by the MOR agonist DAMGO but unaffected by the DOR agonist DPDPE, suggesting expression of MORs but not DORs on thalamic glutamate terminals in the ACC (**Figure 4b-c**, and **figure 4 – figure supplement 1b-c**; $I_{DAMGO}$: 54.0 ± 5.0 % of baseline, W(17) = 1, $p < 0.001$; $I_{DPDPE}$: 93.4 ± 7.0 %, W(14) = 36, p = 0.312; L2/3; $I_{DAMGO}$: 69.3 ± 3.3 % of baseline, W(15) = 0, $p < 0.001$; $I_{DPDPE}$: 92.9 ± 5.4 %, W(9) = 9, p = 0.129). These oEPSCs were of thalamic origin since track injection of ChR2 dorsal to the thalamus resulted in only sporadic and insignificant oEPSCs in the ACC (**Figure 4 – figure supplement 2**).

Surprisingly, both DAMGO and DPDPE potently inhibited GABA-mediated oIPSCs from the MThal to the ACC pyramidal neurons (**Figure 4e-f** and **figure 4 – figure supplement 1e-f**; $I_{DAMGO}$, 37.9 ± 7.8 % of baseline, W(14) = 0, $p < 0.001$; $I_{DPDPE}$, 47.6 ± 7.9 %, W(11) = 1, $p < 0.01$; $I_{DAMGO}$, 61.2 ± 9.5 % of baseline, W(12) = 1, $p < 0.001$; $I_{DPDPE}$, 62.7 ± 5.4 %, W(10) = 0, $p < 0.01$). Since PV-positive neurons reportedly contribute to feed-forward inhibition of MThal inputs to L5 pyramidal neurons in the ACC (Delevich et al., 2015), opioid modulation of oIPSCs of PV neurons onto L5 pyramidal neurons in the ACC was measured. *PV-cre*$^{+/-}$;*Ai32*$^{+/-}$ mice (Madisen et al., 2015, Hippenmeyer et al., 2005) were used to express ChR2(H134R) in PV neurons, and oIPSCs were recorded from L5 pyramidal neurons (**Figure 5a**). The oIPSCs were potently inhibited by DPDPE but not DAMGO (**Figure 5b-c**; $I_{DAMGO}$: 104.1 ± 6.1 % of baseline,

W (11) = 25, p = 0.998; $I_{DPDPE}$: 44.9 ± 5.7 %, W (15) = 0, p < 0.001), suggesting that DORs were expressed on PV neurons in the ACC.

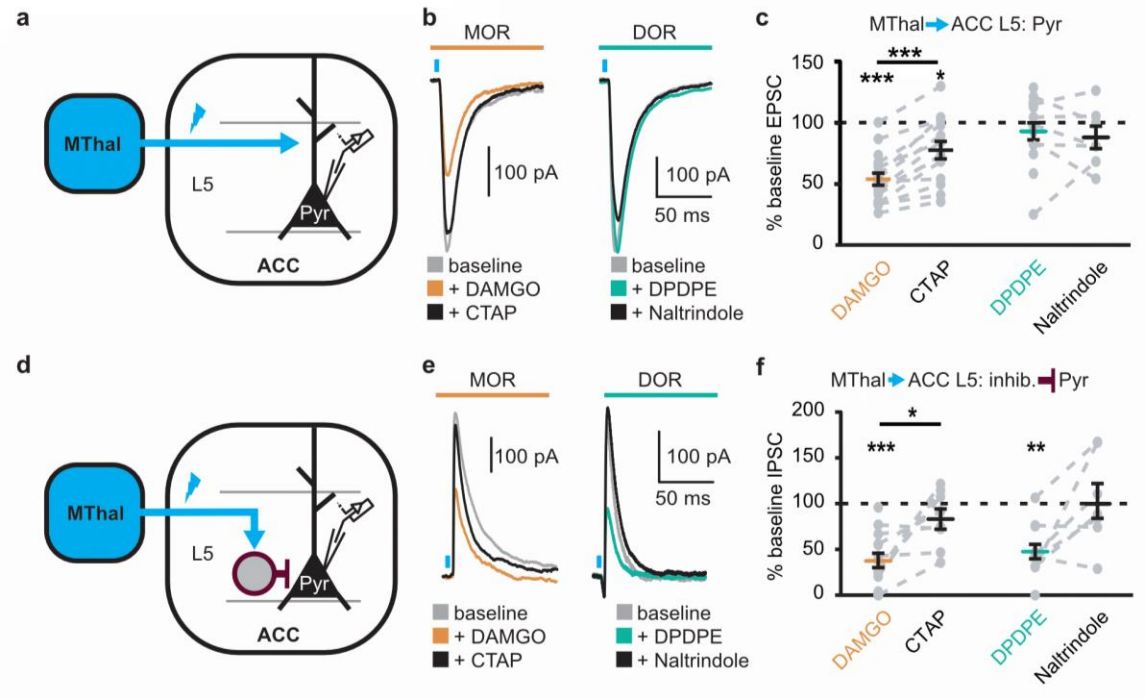


**Figure 4. Mu-opioid agonists suppress thalamic inputs to pyramidal neurons in the ACC while delta-opioid agonists suppress cortical feed-forward inhibition in the ACC**

(**a-c**) oEPSCs of the pyramidal neurons in the ACC elicited by optical stimulation of MThal input. (A) Schematic of ChR2 injection, MThal optical stimulation, and recording of oEPSCs of the layer 5 (L5) pyramidal neurons (Pyr) in the ACC. Blue: ChR2 expression and optical stimulation. (**b**) Example traces of oEPSCs elicited from optical stimulation of the MThal terminals in the ACC during baseline (gray), application of DAMGO (1µM, left panel, orange), followed by CTAP (1 µM, left panel, black), or application of DPDPE (1µM, right panel, teal,) followed by naltrindole (0.3 µM, right panel, black). Blue bars: 1 ms of 470 light stimulation. (**c**) Summary data of oEPSCs of all recording as shown in (**b**) with responses plotted as a percent of the baseline. DAMGO: N = 13, n = 17; CTAP: N = 12, n = 14; *SM* = 22.85, p < 0.001; DPDPE:

N = 11, n = 15; naltrindole: N = 5, n = 7, *SM* = 0.989, p = 0.610. (**d-f**) oIPSCs of the pyramidal neurons from the MThal optical stimulation, via inhibition through interneurons in the ACC. (**d**) Schematic of ChR2 injection, MThal optical stimulation, and recording of the pyramidal neurons in the ACC via feed-forward inhibition. Blue: ChR2 expression and optical stimulation; magenta: outline of an interneuron. (**e**) Example traces of oIPSCs elicited from optical stimulation of the MThal terminals in the ACC during baseline (gray), application of DAMGO (1µM, left panel, orange) followed by CTAP (1 µM, left panel, black), or application of DPDPE (1µM, right panel, teal) followed by naltrindole (0.3 µM, right panel, black). (**f**) Summary data of oIPSCs for all recordings as in (B) with responses plotted as a percent of the baseline. DAMGO: N = 9, n = 14; CTAP, N = 7, n = 8, *SM* = 15.68, p < 0.001; DPDPE: N = 6, n = 12; naltrindole: N = 5, n = 7, *SM* = 7.426, p < 0.05. Skillings-Mack test followed by paired Wilcoxon signed-ranks test *post-hoc* analysis. * p ≤ 0.05; ** p ≤ 0.01; *** p ≤ 0.001. Mean ± standard error of the mean. *SM*: Skillings-Mack statistic; Blue bars: 1 ms of 470 nm light stimulation.

The following figure supplement is available for figure 4:

**Figure supplement 1**. Opioid inhibition of synaptic currents onto layer 2/3 pyramidal neurons in the ACC.

**Figure supplement 2**. Verification of origins of optically-evoked response.

Colocalization of DORs and parvalbumin was investigated at the protein and mRNA levels (**Figure 5d-f**). Images of fluorescent RNA probes for endogenous DORs (*Oprd1*) and parvalbumin (*Pvalb*) revealed that the majority of *Pvalb*-positive cells were also *Oprd1*-positive (**Figure 5d, f**; 88.7 ± 1.4% of *Pvalb*-positive cells expressed detectable levels of *Oprd1*). A knockin mouse line expressing GFP-fused DORs (Scherrer et al., 2006) was used to probe for

the presence of DOR proteins in sections stained for parvalbumin proteins. Similarly, 95.0 ± 1.2% of parvalbumin protein-positive neurons expressed detectable levels of GFP (**Figure 5e-f**). Together, these data indicate that DORs are expressed on PV neurons, consistent with their role in inhibition of GABA release onto pyramidal neurons.

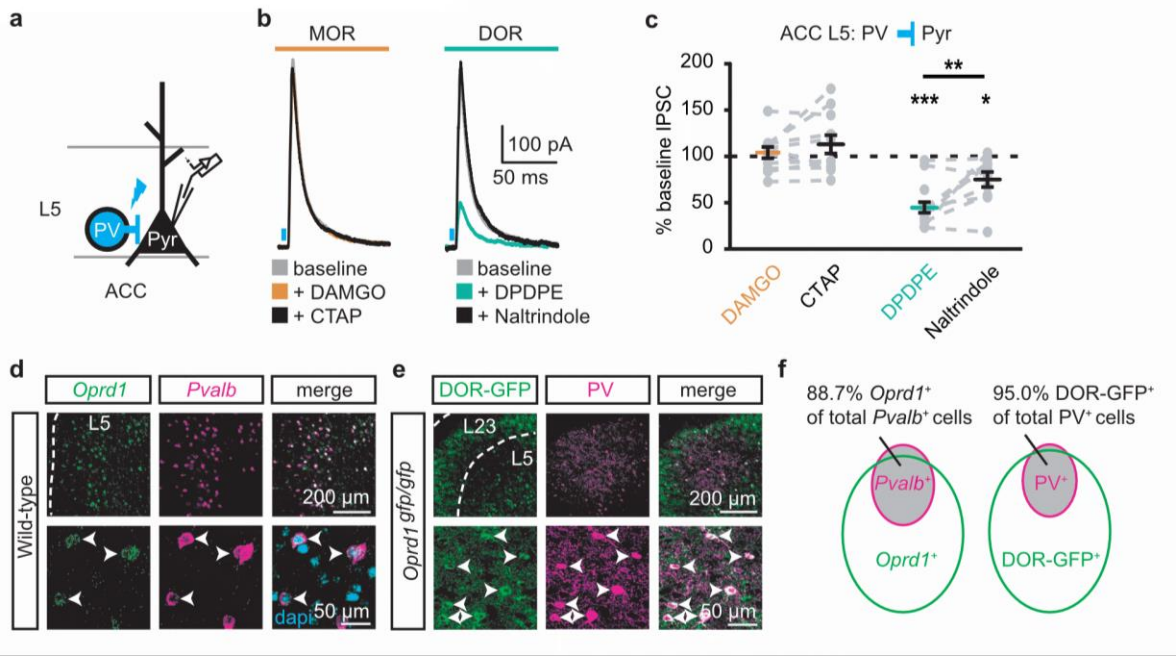


**Figure 5. DORs expressed on PV-positive interneurons suppress oIPSCs onto layer 5 pyramidal neurons**

(**a**) Schematic of ChR2 expression and recording of oIPSCs of parvalbumin-positive interneurons (PV) to layer 5 (L5) pyramidal neurons (Pyr) in the ACC of *PV-cre*$^{+/-}$;*Ai32*$^{+/-}$ mice. Blue: ChR2 expression and optical stimulation. (**b**) Example traces of oIPSCs during baseline (gray), application of DAMGO (1 μM, left panel, orange) and followed by CTAP (1 μM, left panel, black, or application of DPDPE (1 μM, right panel, teal) followed by naltrindole (0.3 μM, right panel, black). (**c**) Summary data of PV interneurons to pyramidal neuron oIPSCs for all recording as in (**b**). Responses plotted as a percent of the baseline. DAMGO/ CTAP: N = 5, n = 11, *SM* = 0.005, p = 0.998; DPDPE: N = 8, n = 15; naltrindole: N = 5, n = 10, *SM* = 19.60, p < 0.001. (**d**) *In-situ* hybridization in wild-type mouse brain sections containing the ACC stained

with probes against mRNA coding for DOR (*Oprd1*, left panel, green) and parvalbumin (*Pvalb*, middle panel, magenta) and overlaid with DAPI (right panel, cyan). (**e**) Immunohistochemistry on the mouse ACC from a *DOR-GFP* knockin mouse and stained with anti-GFP antibodies (left panel, green), and anti-parvalbumin antibodies (middle panel, magenta), and overlaid (right panel). (**f**) Venn diagram quantifying overlap of *Oprd1*-positive and *Pvalb*-positive (left panel, N = 2, n = 8), and DOR-GFP-positive and PV-positive cells in the mouse ACC (right panel, N = 2, n = 15). Skillings-Mack test followed by paired Wilcoxon signed-ranks test *post-hoc* analysis. *, $p < 0.05$; **, $p < 0.01$; *** $p < 0.001$. Mean ± standard error of the mean. *SM*: Skillings-Mack statistic.

**Delta-opioid agonists increase cortical excitability**

As DOR agonists selectively reduced feed-forward inhibition of the local PV neurons to pyramidal neurons in the ACC, activation of DORs was predicted to disinhibit ACC pyramidal neurons resulting in increased cortical excitability. Optical excitation of MThal terminals in the ACC evoked action potential (AP) firing in ACC L5 pyramidal neurons measured using a cell-attached recording configuration (**Figure 6a-c**). When APs were elicited in approximately 50% of the trials, activation of MORs by DAMGO decreased the fraction of trials that evoked action potentials (0.4 ± 0.1 fold change relative to baseline, paired t-test, $p < 0.01$), while activation of DORs by DPDPE led to a significant increase in AP firing probability (5 ± 3.1 fold change relative to baseline, paired t-test, $p < 0.05$). This was consistent with an inhibitory effect of MOR activation and a disinhibitory effect of DOR activation on pyramidal neuron firing rates (**Figure 6b-c**) with no significant effect on action potential latency (**Figure 6 – figure supplement 1**).

359 Thus, DOR activation in the ACC resulted in disinhibition of the pyramidal neurons within the
360 ACC, which led to increased cortical excitability.

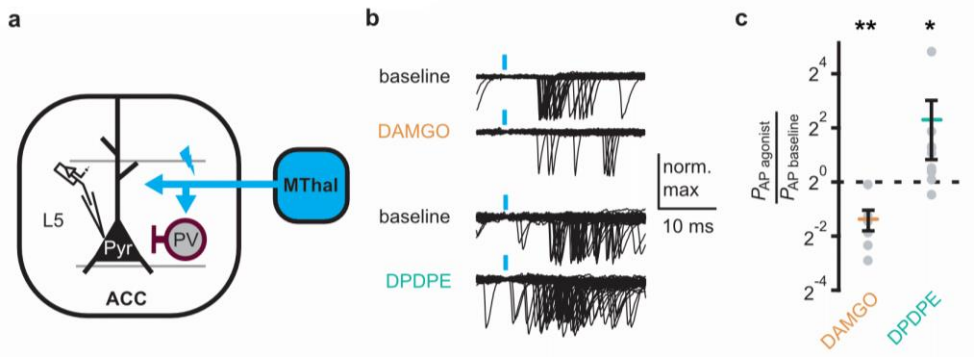


361

362 **Figure 6. DOR activation results in increased cortical excitability**

363 (**a**) Schematic of ChR2 expression and recording of optically-evoked action potentials (APs)
364 using a loose cell-attached recording configuration. Blue: ChR2 expression and optical
365 stimulation; magenta: outline of a parvalbumin -positive interneuron (PV). (**b**) Example traces of
366 50 trails from a single layer 5 (L5) pyramidal neuron (Pyr) in which APs were evoked by optical
367 stimulation (blue bars) under baseline conditions, or in the presence of DAMGO (1 µM, orange),
368 or DPDPE (1 µM, teal). (**c**) Summary data plotted on a log2 scale for action potential firing
369 probability ($P_{AP}$) in the presence of drugs ($P_{AP\ agonist}$) relative to baseline ($P_{AP\ baseline}$). Paired t-test;
370 * $p \leq 0.05$; ** $p \leq 0.01$. DAMGO: N = 3, n = 7; DPDPE: N = 5, n = 8.

371 The following figure supplement is available for figure 6:

372 **Figure supplement 1**. Latencies of thalamocortical-evoked action potentials in ACC pyramidal
373 neurons.

374

375 **Delta-opioid agonists facilitated thalamo-cortico-striatal signaling**

376 The increased excitability upon DOR activation in L5 pyramidal neurons in the ACC was
377 hypothesized to propagate to MSNs in the DMS via corticostriatal projections and result in

increased glutamate release in the striatum. To test this hypothesis, ChR2(H134R) was injected into the MThal. Brain slices containing both the ACC and DMS were prepared (**Figure 7a**). Simultaneous recordings were made from L5 pyramidal neurons in the ACC (voltage recording) and MSNs in the DMS (current recording). Laser illumination was used to focally excite axons within the ACC or the DMS. When the ACC was illuminated, optogenetically stimulated MThal axons triggered action potentials in the L5 pyramidal neurons in the ACC, which then propagated to the DMS, and in turn, triggered a poly-synaptic oEPSCs in the MSNs (**Figure 7a**). In contrast, focal illumination in the DMS resulted in a short latency oEPSC in the MSNs in the DMS with no measurable responses in the L5 pyramidal neurons in the ACC. These results indicated that MThal-ACC-DSM circuits were preserved in this slice preparation. Long-latency poly-synaptic oEPSCs were also confirmed in MSNs in the DMS following widefield optical stimulation of the ACC (**Figure 7b** and **figure 7 – figure supplement 1a**). Application of DPDPE increased the charge transfer of the poly-synaptic MThal→ACC→DMS oEPSCs (**Figure 7b-c**; $Q_{baseline}$: 129.4 ± -46.2 fC; $Q_{DPDPE}$: 344.7 ± 90.5 fC, W (7) = 2, $p < 0.05$). Amplitude changes of the poly-synaptic oEPSC in response to DPDPE, however did not reach statistical significance (**Figure 7 – figure supplement 1b**; $I_{DPDPE}$: 196.1 ± 41.0 %, W (7) = 3, p = 0.145). Taken together, the results indicate the presence of both MORs and DORs in the thalamo-cortico-striatal circuitry, where DORs primarily facilitated information flow in the indirect pathway from the MThal via the ACC to the DMS, while MORs suppressed information flow from the MThal directly to the DMS.

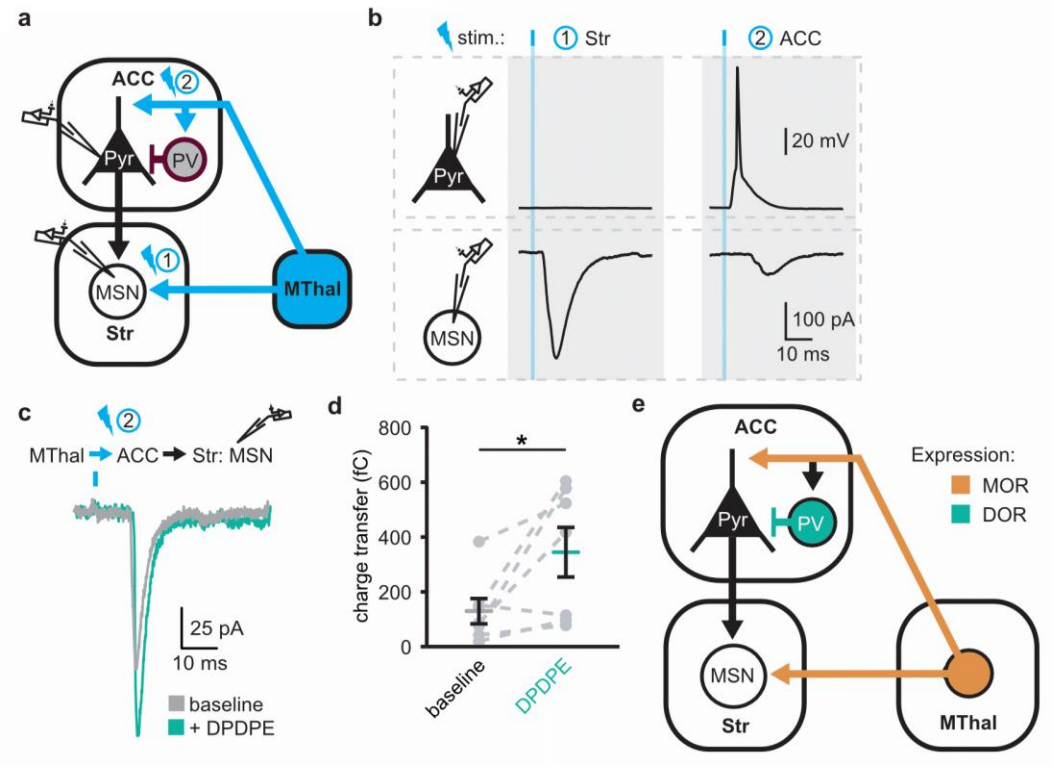


**Figure 7. DOR activation disinhibits thalamo-cortico-striatal circuits.**

(**a**) Schematic of ChR2 expression and dual recordings in layer 5 (L5) pyramidal neurons (Pyr) in the ACC and MSNs in the DMS. Blue: ChR2 expression and optical stimulation; magenta: outline of a parvalbumin-positive interneuron (PV). 470nm light stimulation locations are shown as 1 and 2. (**b**) Example traces of current-clamp recording from a L5 pyramidal neuron in the ACC (upper panels), and voltage-clamp recording from a MSN in the DMS (lower panels) in response to light stimulations at location 1 (Str) and location 2 (ACC). (**c**) Example traces of poly-synaptic current evoked by optical stimulation of MThal terminals in the ACC (location 2) while recording from an MSN in the DMS during baseline (gray), and in presence of DPDPE (1 µm, teal). (**d**) Summary data of the charge transfer of poly-synaptic oEPSCs in the MSNs evoked by optical stimulation of location 2 in the ACC. Paired Wilcoxon signed-ranks test. * $p \leq 0.05$; Gray: baseline; teal: DPDPE. (**e**) Summary schematic depicting a part of the affective and motivational pain circuit consisting of the MThal, ACC and DMS. Str: striatum.

412 The following figure supplement is available for figure 7:

413 **Figure supplement 1**. EPSCs and action potential latencies within the thalamo-cortico-striatal
414 circuits.

415

416 **Discussion**

417 Despite the importance of the thalamo-cortico-striatal loop in affective pain and reward, the
418 exact circuit mechanisms and how they are modulated by opioids are not fully understood.
419 Previously, we described the mesoscopic anatomical connectivity between subregions within the
420 thalamus and cortex, and the convergence of their axonal projections within the striatum
421 (Hunnicutt Elife 2016). Here, guided by such information, we used both anatomical and
422 functional approaches to demonstrate the connectivity of the MThal, ACC and DMS. We found
423 that projections from the MThal and ACC converged in the DMS, rather than the ventral striatum
424 which has been well studied for reward and drug addiction. Further, we found different opioid
425 receptors differentially affect projection-specific synapses (**Figure 7e**). Specifically, activation of
426 MORs suppressed both MThal-ACC and MThal-DMS excitatory synapses, however, activation
427 of DORs enhanced the excitatory input from the MThal to the pyramidal neurons in the ACC by
428 disinhibiting local feed-forward inhibition mediated by PV interneurons in the ACC. This DOR-
429 mediated disinhibition of MThal-ACC synapses has functional significance at the network level
430 in that it facilitates information to flow from the MThal to the DMS via the ACC. Our results
431 suggests that opioid effects on pain and reward are shaped by the relative selectivity of opioid
432 drugs to the specific circuit components.

433

434 **Convergence of thalamic and cortical inputs to the striatum**

Glutamate afferents from the midline cortical structures and medial thalamus converge to the DMS in the affective pain pathway. Here, we demonstrated that single MSNs in the DMS can receive inputs from both the midline cortex and medial thalamus. These results establish the anatomical basis for investigating convergence and integration within this circuit. Being able to detect convergence of MThal and ACC inputs at the level of the individual cell also paves the way for future studies of this circuit with single cell resolution at the population level.

**Individual MThal neurons projects to both the ACC and DMS**

Consistent with studies demonstrating cortical and striatal projections for midline thalamic neurons in rats (Otake and Nakamura, 1998; Kuramoto et al., 2017), the simultaneous retrograde bead injections localized to the rostromedial ACC and DMS demonstrated double-labeling of individual neurons in the lateral MD and CL thalamus, suggesting that single thalamic neurons can project to both the cortex and striatum. It should be acknowledged that the exact location of the retrograde bead labeled neurons relative to defined borders of the thalamic nuclei is not perfectly accurate since a small range of slices containing the MThal were fit to a single plane of the mouse atlas (Franklin & Paxinos, 2001) without correcting for irregularities such as brain slice angles. Furthermore, the diffusion of retrograde beads in brain tissue is limited such that each injection is relatively small and localized, thus, the number of colocalized neurons is not an absolute measure of the fraction of MD neurons projecting to both the ACC and DMS. Despite these constraints, the retrograde bead injections and retrograde viral labeling experiments both suggested the presence of a population of neurons in the MThal that project to both the ACC and DMS. We also confirmed that these collaterals originating from the MThal made functional en passant synapses in the DMS. Based on these tracing experiments and convergence of the

458 cortical and thalamic inputs to the striatum experiments mentioned above, a circuit with a direct
459 monosynaptic arm from the MThal to the DMS, and an indirect poly-synaptic arm from the
460 MThal via ACC to the DMS is described.
461
462 **Opioid modulation of the thalamo-cortico-striatal circuitry**
463 The MOR agonist DAMGO had a strong inhibitory effect on the MThal inputs to the DMS,
464 whereas neither DAMGO nor the DOR agonist DPDPE had a significant effect on the ACC
465 inputs to the DMS. These results indicate that the midline thalamostriatal pathway stands as a
466 major source of opioid-regulated glutamate inputs to the DMS, and that MOR agonists alter the
467 relative influence of cortical and thalamic inputs on DMS excitability. The MThal inputs to the
468 ACC were also inhibited by MOR agonists. Given the extensive MOR-sensitive axonal
469 projections from the MThal to the ACC, it is possible that the analgesic and rewarding effect of
470 morphine injection into the ACC is due in part to inhibition of thalamic glutamate inputs to the
471 ACC (Navratilova et al., 2015). Together, MOR activation may selectively suppress information
472 from MThal to the striatum either directly or indirectly, but may leave intact other information
473 that is also going through the ACC to the striatum. This may contribute to the selective analgesic
474 and rewarding effect of morphine without affecting other cognitive functions.
475
476 **Opposing effects of opioid subtypes on circuitry modulation**
477 Although all opioid receptors couple to the inhibitory $G_i$ pathway, their effect on the circuit can
478 be distinct. In this study, the lack of strong inhibition of DORs on glutamate transmission in the
479 corticostriatal projections together with the potent DOR inhibition of GABA release from PV
480 interneurons to pyramidal neurons in the ACC allows for DORs to function in a disinhibitory

manner. DOR activation effectively leads to hyper-excitable ACC circuits, while MOR activation functions in an inhibitory manner, dampening glutamate release in the thalamo-cortico-striatal circuit. These results complement a previous study in which DOR activation resulted in increased activity in the rat insular cortex following dental pulp stimulation, while MOR activation decreased the insular cortex activity (Yokota, et al., 2016a). A follow-up study found that inhibitory transmission from fast-spiking interneurons to pyramidal neurons was inhibited by DOR activation (Yokota, et al., 2016b). The current results extend these findings to the mouse ACC and identify that specifically, PV interneurons are a target of DOR inhibition.

While PV interneurons have been suggested to selectively mediate feed-forward inhibition of thalamocortical transmission in the ACC, it is important to note that the current findings do not rule out potential influence of opioids on other interneuron populations. In fact, immunohistochemical and *in situ* hybridization data presented here suggest that DOR expression is not restricted to PV interneurons, as only approximately 20% of DOR-positive neurons were parvalbumin-positive (**Figure 4e**). Furthermore, certain neurons in the ACC have been shown to express MORs (Tanaka and North, 1994, Vogt et al., 1995, Wang et al., 2018), suggesting that there are additional opioid-sensitive neurons within the local ACC circuits.

It has recently been shown that MOR agonists can modestly inhibit insular-striatal glutamate transmission (Munoz et al., 2018). In this study ACC-striatal transmission was relatively insensitive to MOR and DOR agonists, while PFC-striatal transmission appeared marginally sensitive to the DOR agonist DPDPE. Thus, there may be heterogeneity in the opioid sensitivity of cortical projections to the striatum. The current results also suggest that MORs and DORs are

504 positioned to serve opposing functions in regulating affective pain circuitry and reward and
505 motivated behaviors.
506
507 The MD, ACC, and striatum have been demonstrated to play roles in pain- and reward-related
508 behaviors (Kawagoe et al., 2007; LaLumiere and Kalivas, 2008; Le Merrer et al., 2009; Harte et
509 al., 2011; Navratilova et al., 2012). Therefore, some aspects of the analgesic and
510 rewarding/addictive effects of opioids may arise from modulation within the poly-synaptic
511 circuits between the MThal, ACC and striatum described here. Increased ACC activity is
512 associated with increased affective pain intensity and decreased ACC activity is associated with
513 analgesia (Johansen and Fields, 2004). The current results suggest that drugs acting in the ACC
514 at either MOR or DOR have the potential to modulate this circuitry. These data also suggest that
515 commonly prescribed and abused opioids, which primarily act through MOR, could alter the
516 relative influences of glutamate inputs to the striatum in addition to their postsynaptic effects on
517 striatal MSNs.
518
519 **Materials and Methods**
520 All procedures were approved by Oregon Health & Science University Institutional Animal Care
521 and Use Committee (IACUC). Mice of both sexes were used in all experiments and were five to
522 eight weeks of age at the time of brain slice preparation. Stereotaxic injections were performed
523 on three- to five-week-old mice. Mice were housed in group housing, given free access to food
524 and water, and maintained on a 12-hour light/ dark cycle. List of resources can be found in table
525 1. The software, and data sets generated and analyzed during the current study are available upon
526 request.

527

528 **Viral Injection**

529 Stereotaxic injections were performed as previously described (Hunnicutt et al., 2014, Birdsong
530 et al., 2015) to deliver recombinant adeno-associated virus (AAV) to express channelrhodopsin
531 variants. Briefly, mice were deeply anesthetized with isofluorane and head fixed into a
532 stereotaxic alignment system (Kopf Instruments, Tujunga, CA, with custom modifications).
533 Small holes were drilled through the skull above the desired injection site and a glass pipette
534 filled with virus was lowered through the hole to the desired injection depth. A small volume (20
535 - 40 nl) of virus was injected (WTB and KAE: Nanoject II, Drummond Scientific, Broomall, PA;
536 BCJ: custom-built injector based on a MO-10, Narishige, Amityville, NY). Injection coordinates
537 are listed below in mm for medial/lateral (M/L), anterior/posterior from bregma (A/P), and
538 dorsal/ ventral from the top of the skull directly over the target area. Target areas included (in
539 mm): medial thalamus (MThal): M/L: 0.55, A/P: -1.2, D/V: 3.6; anteromedial thalamus
540 (AMThal): M/L: 0.55, A/P: -0.4, D/V: 3.4; anterior cingulate cortex (ACC): M/L: 0.4, A/P: 0.7,
541 D/V:1.6; prefrontal cortex (PFC): M/L: 0.45, A/P: 1.75, D/V: 1.6, dorsomedial striatum (DMS);
542 M/L: 1.5; A/P: 0.55, D/V: 3.6 to 3.3.

543

544 **Brain Slice Electrophysiology**

545 Two to three weeks after viral injection, acute brain slices were prepared. Two different slicing
546 protocols were used depending on whether recordings were being obtained from the striatum or
547 ACC. Recordings were made from both slicing solutions and similar results were obtained.

548

For striatal recordings, coronal brain slices (250 - 300 µm) were prepared from either ice-cold or room temperature Krebs buffer containing (in mM): 125 NaCl, 21.4 $NaHCO_3$, 11.1 D-glucose, 2.5 KCl, 1.2 $MgCl_2$, 2.4 $CaCl_2$, 1.2 $NaH_2PO_4$, ~305 mOsm, supplemented with 5 µM MK-801 and saturated with 95% $O_2$/5% $CO_2$. Slices were incubated in oxygenated Krebs buffer supplemented with 10 µM MK-801 for 30 minutes at 33 ºC and then maintained in a holding chamber at 22 – 24 ºC.

For cortical recordings, coronal brain slices (300 – 350 µm) were prepared in a carbogen saturated choline-based cutting solution containing (in mM): 110 choline chloride, 25 $NaHCO_3$, 25 glucose, 2.5 KCl, 7 $MgCl_2$, 0.5 $CaCl_2$, 1.25 $NaH_2PO_4$, 11.5 sodium ascorbate, and 3 sodium pyruvate, ~315 mOsm. Slices were incubated in oxygenated artificial cerebrospinal fluid (aCSF) containing (in mM): 127 NaCl, 25 $NaHCO_3$, 25 D-glucose, 2.5 KCl, 1 $MgCl_2$, 2 $CaCl_2$, and 1.25 $NaH_2PO_4$ for 30 minutes at 33 – 34 ºC and then maintained in a holding chamber at 22 – 24 ºC.

Two experimenters (WTB and BCJ) using two rigs performed whole-cell recordings; experimenters' initials below note differences between experimental setups. There were no differences in results between experimenters so all data were pooled. Recordings were obtained at near-physiological temperature (32 - 34 ºC) from slices superfused with (BCJ) oxygenated aCSF supplemented with (in µM, see table 1): 10 $GABA_B$-receptor antagonist CGP 52432, 10 $GABA_A$-receptor antagonist SR-95531, 10 nicotinic acetylcholine receptor Mecamylamine, 10 muscarinic acetylcholine receptor antagonist Scopolamine, 0.3 metabotropic glutamate receptor 5 antagonist MPEP, 5 NMDA receptor antagonist CPP, or (WTB) oxygenated Krebs supplemented with (in µM, see table 1): 0.2 $GABA_B$-receptor antagonist CGP 55845, 10

571 $GABA_A$-receptor antagonist picrotoxin, 1 mecamylamine, 0.1 muscarinic acetylcholine receptor
572 antagonist atropine or 0.1 scopolamine and 0.3 MPEP, preincubated in 5 MK-801.
573
574 **Electrophysiology Data Acquisition**
575 Borosilicate pipettes (2.8 – 4 MΩ; Sutter Instruments, Novato, CA) were filled with potassium
576 gluconate-based internal solution (in mM: 110 potassium gluconate, 10 KCl, 15 NaCl, 1.5
577 $MgCl_2$, 10 HEPES, 1 EGTA, 2 $Na_2ATP$, 0.3 $Na_2GTP$, 7.8 phosphocreatine; pH 7.35 – 7.40;
578 ~280 mOsm) for striatal recordings. Putative MSNs were identified by their morphology and
579 stereotypic physiological properties. Evoked excitatory postsynaptic currents (EPSCs) were
580 recorded in whole-cell voltage-clamp mode at -75 mV holding potential.
581
582 To facilitate measurement of both $GABA_A$- and AMPA-mediated currents, cortical recordings
583 were obtained using a low-chloride cesium gluconate solution (in mM: 135 Glucaronic acid, 1
584 EGTA, 1.5 $MgCl_2$, 10 HEPES, 2 Na2ATP, 0.3 GTP, 7.8 $Na_2$ Phosphocreatine, titrated to pH
585 7.35-7.4 with CsOH, ~280 mOsm and 3 QX314 chloride added fresh before experiment) in the
586 absence of $GABA_A$ antagonists. Sodium and chloride reversal-potentials were empirically
587 determined by recording spontaneous EPSCs/IPSCs, isolated by presence of GABAergic or
588 glutamatergic antagonists, respectively, under a range of holding potentials (-90 to 40 mV with 5
589 mV increments each for 1 minute recording duration). oEPSC and oIPSC were recorded at -55
590 and 5 mV, respectively.
591
592 Whole-cell voltage clamp recordings were collected by WTB using an Axopatch 200A amplifier
593 (Molecular Devices, San Jose, CA), digitized at 20 kHz (Instrutech ITC-16, New York, NY), and

recorded (Axograph X software), and by BCJ using an Multiclamp 700B amplifier (Molecular Devices) digitized at 10 kHz and recorded with *Ephus* software (www.ephus.org). Optically evoked currents were elicited by LED illumination through the microscope objective (WTB and BCJ, Olympus, Tokyo, Japan, BX51W with 60X, 1.0 NA water immersion objective, except for polysynaptic circuit activation which utilized a 20X, 0.5 NA water immersion objective), or by laser illumination (473 nm Crystal Laser, Reno, NV) through the microscope objective (BCJ, details see Mao et al., 2011 Neuron). In brief, laser beam position was controlled by galvanometer scanners (Cambridge Technology, Bedford, MA). Beam was passed through an air objective (4 x, 0.16 NA, UPlanApo, Olympus, beam diameter ~8-16 µm). Timing and light power of the laser stimulation was controlled by a TTL-controlled shutter (Uniblitz, Rochester, NY) with typical dwell time 1 ms (up to 5 ms for polysynaptic and loose cell-attached experiments in Figures 6 and 7), and a circular gradient neutral-density filter of 0.04-1.5 optical density (Edmund Optics, Barrington, NJ) set to yield typical 3-5 mW power after objective, respectively. For LED stimulation a TTL-controlled LED driver and 470 nm LED (Thorlabs, Newton, NJ) were used to illuminate the slice directly over the recorded cell generally with ~1mW of power for 0.5 ms or 1 ms, although power was increased or decreased if evoked currents were unusually weak or strong, respectively. For two-wavelength optical excitation, single flashes of 470 nm (1 msec, < 0.5 mW) and 625 nm LEDs (3 ms, 1.4 mW, Thorlabs) were used.

**Electrophysiology Data Analysis**

Data collected by WTB were analyzed either in Axograph or Matlab, data collected by BCJ in *Ephus* were analyzed in Matlab. Pooled data were processed in Matlab and R. All collected data

were analyzed using the same protocols. Peak current amplitude was calculated relative to mean current during 50 ms baseline prior to the stimulus. In three cases the recorded oIPSCs (recorded as positive current) was completely blocked in the presences of DAMGO, yielding a small negative current deflection (residual EPSC-mediated sodium current as a result of imperfect voltage-clamp at the estimated sodium-reversal potential). To calculate agonist effects on the oIPSCs relative to baseline recordings the small negative currents were substituted with a positive current value (0.00001 pA). Signal latencies were calculated between stimulation and 10% of peak current for oEPSCs or peak of action potentials. Charge transfer was calculated by integrating recorded current during a defined time window following photostimulation described below after stimulation and was corrected by baseline charge transfer during a time window measured immediately prior to stimulation. In figure S5C a large portion of "non-responding" cells were observed in experiments from "tail" injected mice (hippocampus + retrosplenial cortex). In order to determine the charge transfer in an unbiased way, we first determined the averaged onset, rise, and decay time of monosynaptic inputs to the recorded cells (thalamic and cortical inputs to the MSNs, thalamic inputs to the L2/3 or L5 pyramidal neurons), and determined the integration time window (averaged rise + decay time) and the time position relative to stimulation (averaged onset time) for individual cell types. These cell type-specific integration time windows and positions allowed us to determine the charge transfer in an unbiased way in both responding and non-responding cells. Charge transfer of polysynaptic currents (**Figure 7C**) were calculated as integrated current between onset and decay time window, both defined as 10% of peak current.

**Retrograde Bead Injection and Tissue Processing**

Red and green RetroBeads (Lumafluor, Durham, NC) were injected similar to viral injections described above with the exception that 100 and 200 nl of RetroBeads were injected into the cortex and striatum, respectively. Five days post-injection, mice were transcardially perfused with phosphate-buffered saline (PBS) followed by 4% formaldehyde in PBS. Brains were dissected and stored overnight in 4% formaldehyde in PBS. Sections containing injection sites were sliced at 100 µm thickness, and sections containing the thalamus were sliced at 50 µm thickness and stained with DAPI (300 nM in PBS) to label nuclei.

**Fluorescent Imaging and Analysis for Retrograde Bead Labeling**

Thalamic sections containing red and green retrobeads were imaged at 20x magnification using three laser lines (405, 488 and 561 nm) on a Yokogawa spinning disk confocal microscope (Carl Zeiss, Oberkochen, Germany). A Z-stack series was acquired with a 0.44 µm optical section thickness, and for each image 3 x 3 tiles with 15% overlap were applied. Laser power and exposure times were identical for all images. Retrobead-labeled cells were manually counted on Imaris 9.0 software (Bitplane) and each slice was recounted twice with consistent exposure settings to generate an average. A cell was counted if at least two punctate fluorescent spots were orthogonally detected directly adjacent to DAPI-labeled nuclei. Colocalization of dual-color spots was quantified using a built-in Imaris function with criteria that red and green-labeled spots must be spaced no more than 8 µm apart.

Subsequent imaging alignment was performed according to the mouse brain atlas (Franklin & Paxinos, 2001), and aligned using Adobe Photoshop and Illustrator. Sections containing the mediodorsal thalamus were aligned to the corresponding mouse brain atlas section (Figure 45,

Franklin & Paxinos, 2001) using the hippocampus, habenula, and third ventricle as landmarks; and red, green, and red/green colocalized cells were hand-traced onto the aligned atlas figure. Injection sites were imaged on a brightfield epifluorescent macroscope (Olympus MVX10) using identical settings, and uniform thresholds were established using fluorescent values from the top 90% brightest pixels (ImageJ). The outline of each injection site was aligned to a representative mouse brain atlas section to view the average injection area (for the ACC, Figure 22 and for the DMS, Figure 28 of the Franklin and Paxinos atlas, second edition (Franklin and Paxinos, 2001).

**Retrograde Viral Cell Labeling**

A 60 nl viral mix containing a 3:1 ratio of AAV2retro-Cre (AAVrg-pmSyn1-EBFP-cre, Addgene) and AAV2-GFP (UNC viral core) was injected into the ACC, and a 90 nl injection of AAV2 FLEX-tdTomato (UNC viral core) was injected in the ipsilateral MThal. Three weeks post-injection, mice were transcardially perfused as described above and brains were sectioned 50 µm thick in PBS the following day.

**Immunohistochemistry and Imaging for Retrograde Viral Cell label**

All incubation steps were performed on a shaker and at room temperature unless otherwise stated. Immediately post-slicing, sections were washed with PBS, and then permeabilized for 20 minutes with 1% Triton X-100 in PBS. Sections were subsequently incubated for 1 hour in blocking solution containing PBS with 1% triton X-100 and 0.5% fish skin gelatin (FSG). Rabbit anti-DsRed (Clontech, Mountain View, CA) and chicken anti-GFP (Invitrogen, Carlsbad, CA) primary antibodies diluted 1:500 in the blocking solution were incubated at 4°C overnight. Secondary antibodies were diluted 1:750 and incubated for 2 hours in the blocking solution.

Sections were stained with 300 nM DAPI for 30 minutes to label nuclei, then mounted on microscope slides and embedded in an aqueous-based mounting solution (Fluoromount, Sigma Aldrich, Saint Louis MO). Imaging conditions are similar to retrograde bead labeling experiments. Red and green axons in the DMS were imaged at 63x using a Zeiss LSM 880 with Airyscan on a single tile with 0.44 µm optical section thickness.

**PV/DOR In Situ Hybridization**

Advanced Cell Diagnostics RNAscope Technology (ACD Bioscience, Newark, CA) was used to quantify cells containing *Oprd1* and *Pvalb* mRNA. Briefly, wild-type mice (five to eight weeks old) were deeply anesthetized with ketamine-xylazine and perfused transcardially with 0.1 M PBS, followed by 4% formaldehyde solution in phosphate buffer (PB). Brain was dissected, cryoprotected in 30% sucrose overnight and then frozen in OCT. Frozen tissue was sectioned at 20 µm, transferred onto Superfrost Plus slides and kept at -80°C. Tissue was thawed from -80°C, washed with PBS at room temperature and subsequently processed according to the manufacturer's protocol. We first pretreated the tissue with solutions from the pretreatment kit to permeabilize the tissue, and then incubated with protease for 30 minutes and the hybridization probes for another 2 hours at 40°C. (Wang et al., 2018)

**PV/ DOR Immunohistochemistry**

A previously described immunostaining protocol was employed (Bardoni et al., 2014; Scherrer et al., 2009). Briefly, five to eight week-old mice were deeply anesthetized with ketamine-xylazine and perfused transcardially with 0.1 M PBS, followed by 4% formaldehyde solution in 0.1 M PB. The brain was dissected, post-fixed for 4 hours at 4°C, and cryoprotected overnight in 30% sucrose in PBS. Frozen brain tissue was then sectioned at 40 µm and incubated with a 5% NDST blocking solution (0.3% Triton X-100 solution in 0.1 M PBS plus with 5% normal donkey

serum) for at least 1 hour. The primary antibody was diluted in the same solution, and incubated with brain sections overnight at 4°C. After washing the primary antibody three times for 5 min with 0.3% Triton X-100 solution in 0.1 M PBS, sections were incubated with secondary antibody solution in 1% NDST solution at room temperature for 2 hours. Sections were then mounted on microscope slides with Fluoromount (Southern Biotech, Birmingham, AL) after washing with PB for three times for 5 min. Images were acquired with a confocal microscope (Leica DM2500, Wetzlar, Germany). The following primary antibodies were used: anti-GFP: Abcam (chicken; 1:1,000); anti-Parvalbumin: Swant (goat; 1:1,000).

**Quantification and Statistical Analysis**

For electrophysiology experiments, to avoid observer-bias all data was quantified using automated custom-written analysis software, followed by manual confirmation. For *in-situ* hybridization experiments, signals were manually counted, and cells displaying 5 or more labeled dots in their cytoplasm were considered positive. All experiments involving conditions (baseline, agonist, antagonist) were first tested with a Skillings-Mack test for significant changes in any of the conditions. Only when a significant change was reported ($\alpha = 0.05$), three Wilcoxon signed-rank tests between combination of conditions was performed, unless stated otherwise. The Skillings-mack test is a non-parametric test, which allows for missing data points (unbalanced design). Dual-channelrhodopsin experiments (Figures 1D and S2H) required a linear mixed model (LMM) since a 3-way ANOVA could not be performed due to unbalanced design. LMM accounted for correlation of measurement within individual cells (random effects). The fixed effects in the LMM were opioid type (mu vs. delta), source (MThal vs. ACC/PFC), condition (baseline vs. agonist vs. antagonist), as well as all interactions referred in the text as

two-way (opioid type x source, opioid type x condition, source x condition) and three-way (opioid type x source x condition). Due to the paucity of observations (n = 7/8) and high number of fixed effects, we relaxed the type I error for the LMM to detect significant trends in interactions ($\alpha = 0.15$). *Post-hoc* analysis of *a priori* hypothesis for specific comparisons were performed using linear combinations based on the LMM ($\alpha = 0.05$). The number of experiments performed with independent mice (N) and recorded neurons or counted slices, in case of *in situ* hybridization or immunohistochemistry, (n) is indicated in the legends. Error bars represent standard error of the mean.

743 Table 1. List of Reagents and Resources used in this study.

| REAGENT or RESOURCE | SOURCE | IDENTIFIER |
|---|---|---|
| **Antibodies** | | |
| Living Colors DsRed Polyclonal Anibody | Takara Bio/Clontech | Cat# 632496<br>RRID: AB_10013483 |
| Anti-GFP chicken IgY fraction | Thermo Fisher | Cat# A10262<br>RRID: AB_2534023 |
| Alexa Fluor 488 goat anti-chicken IgG | Thermo Fisher | Cat# A11039<br>RRID: AB_2534096 |
| Alexa Fluor 594 goat anti-rabbit IgG (H + L) | Thermo Fisher | Cat# A11012<br>RRID: AB_2534079 |
| Anti-parvalbumin goat | Swant | Cat# PVG 214<br>RRID: AB_10000345 |
| Anit-GFP chicken | Abcam | Cat# ab13970<br>RRID: AB_300798 |
| **Virus Strains** | | |
| AAV2-syn-hChR2 (H134R)-EYFP | UNC virus vector core | NA |
| AAV2-syn-hChR2 (H134R)-tdTomato (Mao et al. 2011) | UPenn Vector Core | NA |
| AAV2-syn-ChrimsonR-tdTomato (Klapoetke et al., 2014) | UNC virus vector core | NA |
| AAV2-syn-CsChR-GFP (Klapoetke et al., 2014) | UNC virus vector core | NA |
| AAVrg-pmSyn1-EBFP-cre (Madisen et al., 2015, Tervo et al., 2016) | Addgene | Cat# 51507 |
| AAV2-FLEX-TdTomato | UNC virus vector core | NA |
| AAV2-SSpEMBOL-CBA-GFP | UNC virus vector core | NA |
| AAV1-CAG-hChR2 (H134R)-TdTomato | UPenn Vector Core | NA |
| AAV2-DIO-ChR2 (H134R)-EYFP | UNC virus vector core | NA |
| **Chemicals and Peptides** | | |
| Mecamylamine | R&D Systems/Tocris | Cat# 2843 |
| Scopolamine | Sigma Aldrich | Cat# S1013 |
| SR95531 | Hello Bio | Cat# HB0901 |
| Picrotoxin | Hello Bio | Cat# HB0506 |
| [Met$^5$] Enkephalin | Sigma Aldrich | Cat# M6638 |
| DAMGO | Sigma Aldrich | Cat# E7384 |
| CTAP | R&D Systems/Tocris | Cat# 1560 |
| Naloxone | Abcam | Cat# ab120074 |
| DPDPE | Sigma Aldrich | Cat# E-3888 |
| Naltrindole | Sigma Aldrich | Cat# N-115 |
| ICI 174,864 | R&D Systems/Tocris | Cat# 0820 |
| MK801 | Hello Bio | Cat# HB0004 |
| CPP | R&D Systems/Tocris | Cat# 0173 |
| CGP 55845 | R&D Systems/Tocris | Cat# 1248 |
| Bestatin | Sigma Aldrich | Cat# B8385 |
| Thiorphan | Sigma Aldrich | Cat# T6031 |

| | | |
|---|---|---|
| MPEP | R&D Systems/Tocris | Cat# 1212 |
| Red Retrobeads IX | Lumafluor Inc | Cat# R180 |
| Green Retrobeads IX | Lumafluor Inc | Cat# R180 |
| DNQX | Sigma Aldrich | Cat# D0540 |
| QX314 | R&D Systems/Tocris | Cat# 2313 |
| **Critical Commercial Assays** | | |
| RNAscope Multiplex Fluorescent Assay | Advanced Cell Diagnostics | Cat# 320850 |
| RNAscope® Probe- Mm-Oprd1 | Advanced Cell Diagnostics | Cat# 427371 |
| RNAscope® Probe- Mm-Pvalb-C2 | Advanced Cell Diagnostics | Cat# 421931-C2 |
| **Experimental Models: Strains** | | |
| Mouse: C57BL/6J | Jackson Laboratories | Cat# 000664 RRID: IMSR_JAX:000664 |
| Mouse: Ai32 (B6;129S-*Gt(ROSA)26Sor*$^{tm32(CAG-COP4*H134R/EYFP)}$*Hze*/J) | Jackson Laboratories | Cat# 012569 RRID: IMSR_JAX:012569 |
| Mouse: Ai9 (B6.Cg-Gt(ROSA)26Sor $^{tm9(CAG-tdTomato)}$Hze/J) | Jackson Laboratories | Cat# 007909 RRID: IMSR_JAX: 007909 |
| Mouse: *PV-IRES-Cre (*B6.129P2-Pvalbtm1(cre)Arbr/J*)* | Jackson Laboratories | Cat# 008069 RRID: IMSR_JAX: 008069 |
| Mouse: *vGlut2-IRES-Cre* | Jackson Laboratories | Cat# 016963 RRID: IMSR_JAX: 016963 |
| **Software** | | |
| FIJI 1.49b | Wayne Rasband, NIH | |
| AxoGraph 1.4.4 | Axograph | |
| Microsoft Excel 2011 | Microsoft Corp. | |
| Illustrator CS5 | Adobe Systems | |
| Photoshop CS5 | Adobe Systems | |
| Prism 6 | GraphPad | |
| Imaris | Bitplane | |
| Zen | Zeiss | |
| Chart 5 | AD Instruments | |
| Matlab r2007b and r2018a | Mathworks | |
| R (3.5.0) | R Development Core Team | |
| Ephus | Vidrio Technologies, LLC | |

## Acknowledgements:

We would like to thank Dr. John Williams for providing guidance and financial support to W.T. B. (NIH R01DA08136), and Dr. Emmeke Aarts and Sheila Markwardt M.P.H. for providing guidance and comments on the statistical analyses. We thank Drs. John Williams, Haining Zhong, and Brooks Robinson for comments to the manuscript. This work was supported by NIH

grants R01DA042779 (W.T.B.), R01DA044481 (G.S.), R01NS106301 (G.S.), R01NS081071 (T.M.) and U01NS094247 (T.M.), R01NS104944 (T.M.), and the New York Stem Cell Foundation (G.S.).

**Author Contributions:**

Conceptualization: W.T.B., B.C.J., T.M.; Methodology W.T.B., B.C.J, K.A.E, D.W., G.S., T.M; Software, B.C.J; Formal Analysis, B.C.J. and W.T.B.; Investigation, W.T.B, B.C.J, K.A.E, D.W.; Resources, W.T.B., G.S., T.M.; Data Curation, B.C.J., Writing-Original Draft, W.T.B. and B.C.J., Writing-Reviewing & Editing, W.T.B., B.C.J, K.A.E., D.W., G.S., T.M., Visualization, B.C.J, W.T.B, K.A.E, D.W; Supervision, W.T.B, G.S, T.M, Funding Acquisition, W.T.B, G.S, T.M.

**The authors declare no competing interests.**

## References

Ananthan, S., 2008. Opioid ligands with mixed μ/δ opioid receptor interactions: an emerging approach to novel analgesics. In *Drug Addiction* (pp. 367-380). Springer, New York, NY.

Atwood, B.K., Kupferschmidt, D.A. and Lovinger, D.M., (2014). Opioids induce dissociable forms of long-term depression of excitatory inputs to the dorsal striatum. *Nature neuroscience*, *17*(4), p.540.

Ballantine Jr, H.T., Cassidy, W.L., Flanagan, N.B. and Marino Jr, R., (1967). Stereotaxic anterior cingulotomy for neuropsychiatric illness and intractable pain. *Journal of neurosurgery*, *26*(5), pp.488-495.

Banghart, M.R., Neufeld, S.Q., Wong, N.C. and Sabatini, B.L., (2015). Enkephalin disinhibits mu opioid receptor-rich striatal patches via delta opioid receptors. *Neuron*, *88*(6), pp.1227-1239.

Bantick, S.J., Wise, R.G., Ploghaus, A., Clare, S., Smith, S.M. and Tracey, I., (2002). Imaging how attention modulates pain in humans using functional MRI. *Brain*, *125*(2), pp.310-319.

Bardoni, R., Tawfik, V.L., Wang, D., François, A., Solorzano, C., Shuster, S.A., Choudhury, P., Betelli, C., Cassidy, C., Smith, K. and de Nooij, J.C., (2014). Delta opioid receptors presynaptically regulate cutaneous mechanosensory neuron input to the spinal cord dorsal horn. *Neuron*, *81*(6), pp.1312-1327.

Berendse, H.W. and Groenewegen, H.J., (1990). Organization of the thalamostriatal projections in the rat, with special emphasis on the ventral striatum. *Journal of Comparative Neurology*, *299*(2), pp.187-228.

Birdsong, W.T., Arttamangkul, S., Bunzow, J.R. and Williams, J.T., 2015. Agonist binding and desensitization of the mu-opioid receptor is modulated by phosphorylation of the C-terminal tail domain. *Molecular pharmacology*, pp.mol-114.

Boyden, E.S., Zhang, F., Bamberg, E., Nagel, G. and Deisseroth, K., (2005). Millisecond-timescale, genetically targeted optical control of neural activity. *Nature neuroscience*, *8*(9), p.1263.

Brundege, J.M. and Williams, J.T., (2002). Differential modulation of nucleus accumbens synapses. *Journal of Neurophysiology*, *88*(1), pp.142-151.

Cahill, C.M., Morinville, A., Hoffert, C., O'donnell, D. and Beaudet, A., (2003). Up-regulation and trafficking of δ opioid receptor in a model of chronic inflammation: implications for pain control. *Pain*, *101*(1-2), pp.199-208.

Carr, K.D. and Bak, T.H., (1988). Medial thalamic injection of opioid agonists: μ-agonist increases while κ-agonist decreases stimulus thresholds for pain and reward. *Brain research*, *441*(1-2), pp.173-184.

Casey, K.L., Minoshima, S., Berger, K.L., Koeppe, R.A., Morrow, T.J. and Frey, K.A., (1994). Positron emission tomographic analysis of cerebral structures activated specifically by repetitive noxious heat stimuli. *Journal of Neurophysiology*, *71*(2), pp.802-807.

Corder, G., Castro, D.C., Bruchas, M.R. and Scherrer, G., 2018. Endogenous and exogenous opioids in pain. *Annual review of neuroscience*, Jul 8, (41), pp 453-473

Cui, Y., Ostlund, S.B., James, A.S., Park, C.S., Ge, W., Roberts, K.W., Mittal, N., Murphy, N.P., Cepeda, C., Kieffer, B.L. and Levine, M.S., (2014). Targeted expression of μ-opioid receptors in a subset of striatal direct-pathway neurons restores opiate reward. *Nature neuroscience*, *17*(2), p.254.

Davis, K.D., Taylor, S.J., Crawley, A.P., Wood, M.L. and Mikulis, D.J., (1997). Functional MRI of pain-and attention-related activations in the human cingulate cortex. *Journal of Neurophysiology*, *77*(6), pp.3370-3380.

Delevich, K., Tucciarone, J., Huang, Z.J. and Li, B., (2015). The mediodorsal thalamus drives feedforward inhibition in the anterior cingulate cortex via parvalbumin interneurons. *Journal of Neuroscience*, *35*(14), pp.5743-5753.

Ding, J., Peterson, J.D. and Surmeier, D.J., (2008). Corticostriatal and thalamostriatal synapses have distinctive properties. *Journal of Neuroscience*, *28*(25), pp.6483-6492.

Erbs, E., Faget, L., Scherrer, G., Matifas, A., Filliol, D., Vonesch, J.L., Koch, M., Kessler, P., Hentsch, D., Birling, M.C. and Koutsourakis, M., (2015). A mu–delta opioid receptor brain atlas reveals neuronal co-occurrence in subcortical networks. *Brain Structure and Function*, *220*(2), pp.677-702.

Fields, H.L., 2004. State-dependent opioid control of pain. *Nature Reviews Neuroscience*, *5*(7), p.565.

Franklin, K.B. and Paxinos, G., 2001. *The Mouse Brain in Stereotaxic Coordinates* San Diego: Academic Press.

Gracely, R.H., 1992. Affective dimensions of pain How many and how measured?. *APS Journal*, *1*(4), pp.243-247.

Guo, N., Garcia, M.M., Taylor, B.K., Zadina, J.E. and Harlan, R.E., (2008). Blockade of mu-opioid receptors in the medial thalamus inhibits acquisition, but not expression, of morphine-induced conditioned place preference. *Neuroscience*, *151*(4), pp.948-954.

Harte, S.E., Spuz, C.A. and Borszcz, G.S., (2011). Functional interaction between medial thalamus and rostral anterior cingulate cortex in the suppression of pain affect. *Neuroscience*, *172*, pp.460-473.

Hippenmeyer, S., Vrieseling, E., Sigrist, M., Portmann, T., Laengle, C., Ladle, D.R. and Arber, S., 2005. A developmental switch in the response of DRG neurons to ETS transcription factor signaling. *PLoS biology*, *3*(5), p.e159.

Hoffman, A.F. and Lupica, C.R., (2001). Direct actions of cannabinoids on synaptic transmission in the nucleus accumbens: a comparison with opioids. *Journal of neurophysiology*, *85*(1), pp.72-83.

Huerta-Ocampo, I., Mena-Segovia, J. and Bolam, J.P., (2014). Convergence of cortical and thalamic input to direct and indirect pathway medium spiny neurons in the striatum. *Brain Structure and Function*, *219*(5), pp.1787-1800.

Hunnicutt, B.J., Long, B.R., Kusefoglu, D., Gertz, K.J., Zhong, H. and Mao, T., 2014. A comprehensive thalamocortical projection map at the mesoscopic level. *Nature neuroscience*, *17*(9), p.1276.

Hunnicutt, B.J., Jongbloets, B.C., Birdsong, W.T., Gertz, K.J., Zhong, H. and Mao, T., (2016). A comprehensive excitatory input map of the striatum reveals novel functional organization. *Elife*, *5*.

Jiang, Z.G. and North, R.A., (1992). Pre-and postsynaptic inhibition by opioids in rat striatum. *Journal of Neuroscience*, *12*(1), pp.356-361.

Johansen, J.P., Fields, H.L. and Manning, B.H., (2001). The affective component of pain in rodents: direct evidence for a contribution of the anterior cingulate cortex. *Proceedings of the National Academy of Sciences*, *98*(14), pp.8077-8082.

Johansen, J.P. and Fields, H.L., 2004. Glutamatergic activation of anterior cingulate cortex produces an aversive teaching signal. *Nature neuroscience*, *7*(4), p.398.

Kawagoe, T., Tamura, R., Uwano, T., Asahi, T., Nishijo, H., Eifuku, S. and Ono, T., (2007). Neural correlates of stimulus–reward association in the rat mediodorsal thalamus. *Neuroreport*, *18*(7), pp.683-688.

Klapoetke, N.C., Murata, Y., Kim, S.S., Pulver, S.R., Birdsey-Benson, A., Cho, Y.K., Morimoto, T.K., Chuong, A.S., Carpenter, E.J., Tian, Z. and Wang, J., (2014). Independent optical excitation of distinct neural populations. *Nature methods*, *11*(3), p.338.

Koshimizu, Y., Wu, S.X., Unzai, T., Hioki, H., Sonomura, T., Nakamura, K.C., Fujiyama, F. and Kaneko, T., 2008. Paucity of enkephalin production in neostriatal striosomal neurons: analysis with preproenkephalin–green fluorescent protein transgenic mice. *European Journal of Neuroscience*, *28*(10), pp.2053-2064.

Kreitzer, A.C., (2009). Physiology and pharmacology of striatal neurons. *Annual review of neuroscience*, *32*, pp.127-147.

Kuramoto, E., Pan, S., Furuta, T., Tanaka, Y.R., Iwai, H., Yamanaka, A., Ohno, S., Kaneko, T., Goto, T. and Hioki, H., (2017). Individual mediodorsal thalamic neurons project to multiple areas of the rat prefrontal cortex: A single neuron-tracing study using virus vectors. *Journal of Comparative Neurology*, *525*(1), pp.166-185.

LaLumiere, R.T. and Kalivas, P.W., (2008). Glutamate release in the nucleus accumbens core is necessary for heroin seeking. *Journal of Neuroscience*, *28*(12), pp.3170-3177.

Le Merrer, J., Becker, J.A., Befort, K. and Kieffer, B.L., (2009). Reward processing by the opioid system in the brain. *Physiological reviews*, *89*(4), pp.1379-1412.

Madisen, L., Garner, A.R., Shimaoka, D., Chuong, A.S., Klapoetke, N.C., Li, L., van der Bourg, A., Niino, Y., Egolf, L., Monetti, C. et al., (2015). Transgenic mice for intersectional targeting of neural sensors and effectors with high specificity and performance. *Neuron*, *85*(5), pp.942-958.

Mansour, A., Fox, C.A., Burke, S., Meng, F., Thompson, R.C., Akil, H. and Watson, S.J., (1994). Mu, delta, and kappa opioid receptor mRNA expression in the rat CNS: an in situ hybridization study. *Journal of Comparative Neurology*, *350*(3), pp.412-438.

Mao, T., Kusefoglu, D., Hooks, B.M., Huber, D., Petreanu, L. and Svoboda, K., 2011. Long-range neuronal circuits underlying the interaction between sensory and motor cortex. *Neuron*, *72*(1), pp.111-123.

Matthes, H.W., Maldonado, R., Simonin, F., Valverde, O., Slowe, S., Kitchen, I., Befort, K., Dierich, A., Le Meur, M., Dollé, P. and Tzavara, E., (1996). Loss of morphine-induced analgesia, reward effect and withdrawal symptoms in mice lacking the μ-opioid-receptor gene. *Nature*, *383*(6603), p.819.

McAlonan, G.M., Robbins, T.W. and Everitt, B.J., (1993). Effects of medial dorsal thalamic and ventral pallidal lesions on the acquisition of a conditioned place preference: further evidence for the involvement of the ventral striatopallidal system in reward-related processes. *Neuroscience*, *52*(3), pp.605-620.

Miura, M., Saino-Saito, S., Masuda, M., Kobayashi, K. and Aosaki, T., (2007). Compartment-specific modulation of GABAergic synaptic transmission by μ-opioid receptor in the mouse striatum with green fluorescent protein-expressing dopamine islands. *Journal of Neuroscience*, *27*(36), pp.9721-9728.

Muñoz, B., Fritz, B.M., Yin, F. and Atwood, B.K., (2018). Alcohol exposure disrupts mu opioid receptor-mediated long-term depression at insular cortex inputs to dorsolateral striatum. *Nature communications*, *9*(1), p.1318.

Nagel, G., Brauner, M., Liewald, J.F., Adeishvili, N., Bamberg, E. and Gottschalk, A., (2005). Light activation of channelrhodopsin-2 in excitable cells of Caenorhabditis elegans triggers rapid behavioral responses. *Current Biology*, *15*(24), pp.2279-2284.

Navratilova, E., Xie, J.Y., Okun, A., Qu, C., Eyde, N., Ci, S., Ossipov, M.H., King, T., Fields, H.L. and Porreca, F., (2012). Pain relief produces negative reinforcement through activation of mesolimbic reward–valuation circuitry. *Proceedings of the National Academy of Sciences*, *109*(50), pp.20709-20713.

Navratilova, E., Xie, J.Y., Meske, D., Qu, C., Morimura, K., Okun, A., Arakawa, N., Ossipov, M., Fields, H.L. and Porreca, F., (2015). Endogenous opioid activity in the anterior cingulate cortex is required for relief of pain. *Journal of Neuroscience*, *35*(18), pp.7264-7271.

Navratilova, E., Atcherley, C.W. and Porreca, F., (2015). Brain circuits encoding reward from pain relief. *Trends in neurosciences*, *38*(11), pp.741-750.

Oertel, B.G., Preibisch, C., Wallenhorst, T., Hummel, T., Geisslinger, G., Lanfermann, H. and Lötsch, J., 2008. Differential opioid action on sensory and affective cerebral pain processing. *Clinical Pharmacology & Therapeutics*, *83*(4), pp.577-588.

Otake, K. and Nakamura, Y., (1998). Single midline thalamic neurons projecting to both the ventral striatum and the prefrontal cortex in the rat. *Neuroscience*, *86*(2), pp.635-649.

Parnaudeau, S., O'Neill, P.K., Bolkan, S.S., Ward, R.D., Abbas, A.I., Roth, B.L., Balsam, P.D., Gordon, J.A. and Kellendonk, C., (2013). Inhibition of mediodorsal thalamus disrupts thalamofrontal connectivity and cognition. *Neuron*, *77*(6), pp.1151-1162.

Pert, C.B., Kuhar, M.J. and Snyder, S.H., 1976. Opiate receptor: autoradiographic localization in rat brain. *Proceedings of the national academy of Sciences*, *73*(10), pp.3729-3733.

Peyron, R., García-Larrea, L., Grégoire, M.C., Costes, N., Convers, P., Lavenne, F., Mauguière, F., Michel, D. and Laurent, B., (1999). Haemodynamic brain responses to acute pain in humans: sensory and attentional networks. *Brain*, *122*(9), pp.1765-1780.

Peyron, R., Laurent, B. and Garcia-Larrea, L., (2000). Functional imaging of brain responses to pain. A review and meta-analysis (2000). *Neurophysiologie Clinique/Clinical Neurophysiology*, *30*(5), pp.263-288.

Pradhan, A.A., Befort, K., Nozaki, C., Gavériaux-Ruff, C. and Kieffer, B.L., (2011). The delta opioid receptor: an evolving target for the treatment of brain disorders. *Trends in pharmacological sciences*, *32*(10), pp.581-590.

Price, D.D., (2000). Psychological and neural mechanisms of the affective dimension of pain. *Science*, *288*(5472), pp.1769-1772.

Rainville, P., Duncan, G.H., Price, D.D., Carrier, B. and Bushnell, M.C., (1997). Pain affect encoded in human anterior cingulate but not somatosensory cortex. *Science*, *277*(5328), pp.968-971.

Scherrer, G., Tryoen-Tóth, P., Filliol, D., Matifas, A., Laustriat, D., Cao, Y.Q., Basbaum, A.I., Dierich, A., Vonesh, J.L., Gavériaux-Ruff, C. and Kieffer, B.L., 2006. Knockin mice expressing fluorescent δ-opioid receptors uncover G protein-coupled receptor dynamics in vivo. *Proceedings of the National Academy of Sciences*, *103*(25), pp.9691-9696.

Scherrer, G., Imamachi, N., Cao, Y.Q., Contet, C., Mennicken, F., O'Donnell, D., Kieffer, B.L. and Basbaum, A.I., (2009). Dissociation of the opioid receptor mechanisms that control mechanical and heat pain. *Cell*, *137*(6), pp.1148-1159.

Tanaka, E. and North, R.A., (1994). Opioid actions on rat anterior cingulate cortex neurons in vitro. *Journal of Neuroscience*, *14*(3), pp.1106-1113.

Tervo, D.G.R., Hwang, B.Y., Viswanathan, S., Gaj, T., Lavzin, M., Ritola, K.D., Lindo, S., Michael, S., Kuleshova, E., Ojala, D. et al., (2016). A designer AAV variant permits efficient retrograde access to projection neurons. *Neuron*, *92*(2), pp.372-382.

Treede, R.D., Kenshalo, D.R., Gracely, R.H. and Jones, A.K., 1999. The cortical representation of pain. *Pain*, *79*(2-3), pp.105-111.

Vogt, B.A., Finch, D.M. and Olson, C.R., (1992). Functional heterogeneity in cingulate cortex: the anterior executive and posterior evaluative regions. *Cerebral cortex*, *2*(6), pp.435-443.

Vogt, B.A., Wiley, R.G. and Jensen, E.L., (1995). Localization of mu and delta opioid receptors to anterior cingulate afferents and projection neurons and input/output model of mu regulation. *Experimental neurology*, *135*(2), pp.83-92.

Vong, L., Ye, C., Yang, Z., Choi, B., Chua, S. and Lowell, B.B., (2011). Leptin action on GABAergic neurons prevents obesity and reduces inhibitory tone to POMC neurons. *Neuron*, *71*(1), pp.142-154.

Wang, D., Tawfik, V.L., Corder, G., Low, S.A., François, A., Basbaum, A.I. and Scherrer, G., (2018). Functional Divergence of Delta and Mu Opioid Receptor Organization in CNS Pain Circuits. *Neuron*.

Whitt, J.L., Masri, R., Pulimood, N.S. and Keller, A., (2013). Pathological activity in mediodorsal thalamus of rats with spinal cord injury pain. *Journal of Neuroscience*, *33*(9), pp.3915-3926.

Williams, J.T., Ingram, S.L., Henderson, G., Chavkin, C., von Zastrow, M., Schulz, S., Koch, T., Evans, C.J. and Christie, M.J., (2013). Regulation of μ-opioid receptors: desensitization, phosphorylation, internalization, and tolerance. *Pharmacological reviews*, *65*(1), pp.223-254.

Wu, Y.W., Kim, J.I., Tawfik, V.L., Lalchandani, R.R., Scherrer, G. and Ding, J.B., (2015). Input-and cell-type-specific endocannabinoid-dependent LTD in the striatum. *Cell reports*, *10*(1), pp.75-87.

Yen, C.P., Kung, S.S., Su, Y.F., Lin, W.C., Howng, S.L. and Kwan, A.L., (2005). Stereotactic bilateral anterior cingulotomy for intractable pain. *Journal of clinical neuroscience*, *12*(8), pp.886-890.

Yokota, E., Koyanagi, Y., Yamamoto, K., Oi, Y., Koshikawa, N. and Kobayashi, M., (2016). Opioid subtype-and cell-type-dependent regulation of inhibitory synaptic transmission in the rat insular cortex. *Neuroscience*, *339*, pp.478-490.

Yokota, E., Koyanagi, Y., Nakamura, H., Horinuki, E., Oi, Y. and Kobayashi, M., (2016). Opposite effects of mu and delta opioid receptor agonists on excitatory propagation induced in rat somatosensory and insular cortices by dental pulp stimulation. *Neuroscience letters*, *628*, pp.52-58.

Zhang, Z., Gadotti, V.M., Chen, L., Souza, I.A., Stemkowski, P.L. and Zamponi, G.W., (2015). Role of prelimbic GABAergic circuits in sensory and emotional aspects of neuropathic pain. *Cell reports*, *12*(5), pp.752-759.

Zubieta, J.K., Smith, Y.R., Bueller, J.A., Xu, Y., Kilbourn, M.R., Jewett, D.M., Meyer, C.R., Koeppe, R.A. and Stohler, C.S., (2001). Regional mu opioid receptor regulation of sensory and affective dimensions of pain. *Science*, *293*(5528), pp.311-315.

## Supplemental figures

### Figure 1 – figure supplement 1

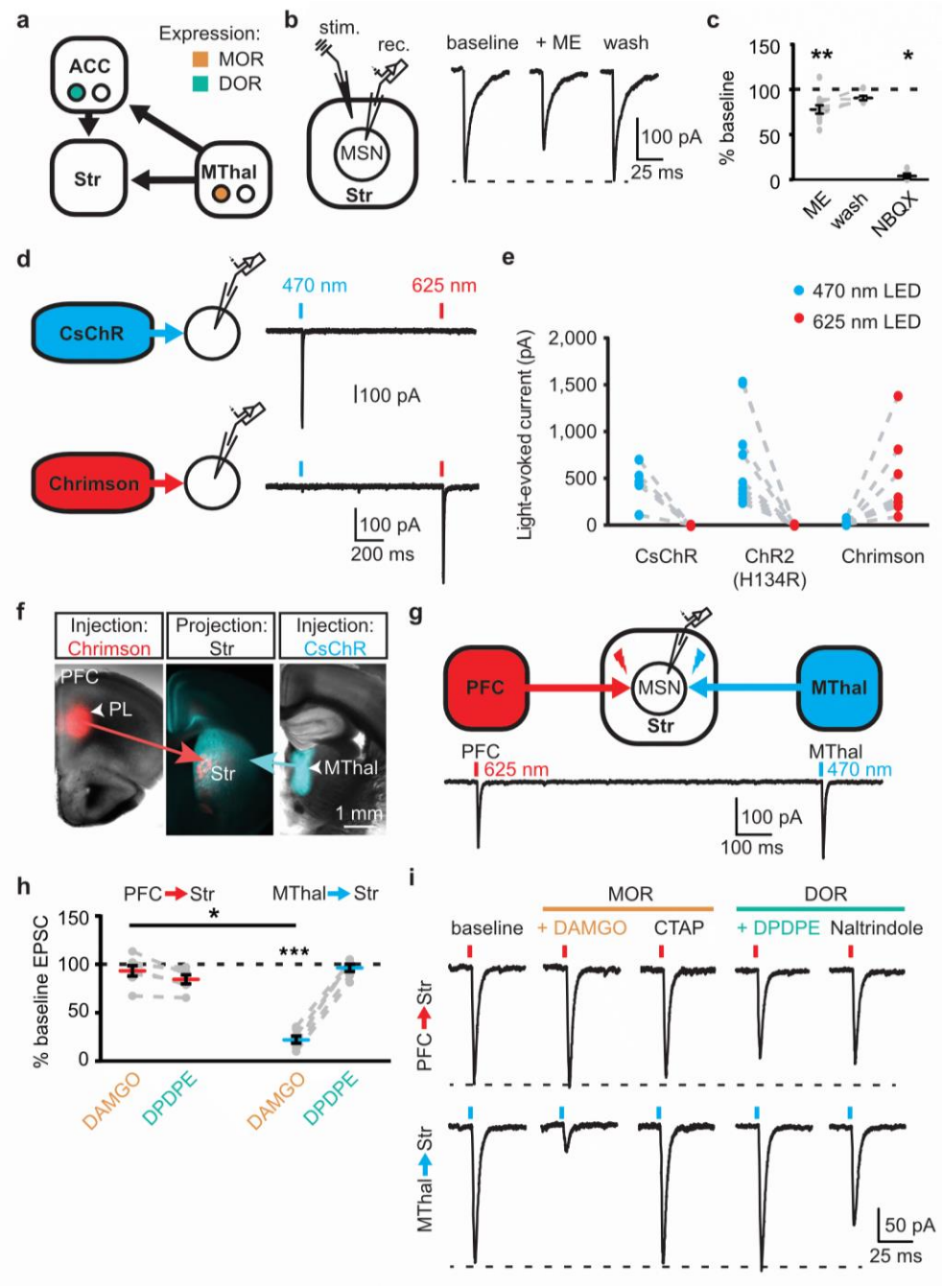


**Mu-opioid agonists suppress thalamic, but not cortical inputs.**

(A) Schematic of thalamo-cortico-striatal circuits and putative expression pattern of MORs (orange) and DORs (teal) (Erbs et al. 2015, Hunnicutt et al. 2016). (B) Schematic and example

traces of electrically-evoked EPSCs from a MSN in the DMS. ME: non-selective opioid agonist [Met$^5$]-enkephalin (3 µM). (C) Summary data of opioid inhibition of EPSCs, as shown in panel B, plotted as a percent of peak current in the drug condition relative to the baseline. ME: N = 6, n = 11; wash: N = 3, n = 6, *SM* = 9.712, $p < 0.01$; baseline vs. ME: W(11) = 1, $p < 0.01$; baseline vs. wash: W(6) = 1, $p = 0.063$; NBQX: N = 4, n = 5; baseline vs. NBQX: W(5) = 0, $p < 0.05$. (D) Independent activation of CsChR and Chrimson using two-wavelength optical excitation. CsChR (blue): virus expressing CsChR injected into the MThal; Chrimson (red): virus expressing Chrimson injected into the ACC. Blue bars: optical excitation with 470 nm light (1 ms, 0.5 mW); red bars: 625 nm light (3 ms, 1.4 mW). (E) Quantification of spectral selectivity of CsChR, ChR2(H134R), and Chrimson plotted as peak optically-evoked EPSC (oEPSC) amplitude following 470 nm (blue) or 625 nm (red) LED optical excitation (CsChR: N = 2, n = 5, $I_{625nm}$:$I_{470nm}$ = -.0002 ± .0081, paired t-test $p < 0.01$; ChR2 (H134R): N = 4, n = 10, $I_{625nm}$:$I_{470nm}$ = 0.0009 ± .002, paired t-test $p < 0.01$: Chrimson: N = 5, n = 8, $I_{470nm}$:$I_{625nm}$ = 0.0423 ± 0.014, paired t-test $p < 0.05$). (F) Overlaid brightfield and epifluorescent images of coronal brain slices showing expression of CsChR in the MThal and axonal projections to the DMS (blue), and expression of Chrimson (red) in the PFC and axonal projections to the DMS (red). (G) Two-wavelength optical excitation elicited oEPSCs in response to 470 and 625 nm light in single MSNs when CsChR was injected into the MThal and Chrimson was injected into the PFC. (H) Summary data of DAMGO (1 µM, orange) and DPDPE (1 µM, teal) effects on oEPSCs elicited from the MThal (blue) and PFC (red) using two-wavelength optical excitation protocol. Linear mixed model: 3-way interaction; opioid type (mu vs. delta opioid) x source (PFC vs. MThal) x condition (baseline vs. agonist vs. antagonist): F(4,7) = 2.171, $p = 0.174$, N = 5, n = 7; DAMGO: $I_{MThal}$; 22.2 ± - 3.6 % of baseline, $z = 3.497$, $p < 0.001$, $I_{PFC}$; 93.9 ± 5.6 %, $z = 0.052$, $p = 0.958$;

DPDPE: $I_{MThal}$; 96.4 ± 3.9 % of baseline, $z$ = 0.087, p = 0.931; $I_{PFC}$: 81.6 ±3.9 %, $z$ = 0.672, p = 0.502. $MThal_{baseline\ x\ DAMGO}$ vs. $ACC_{baseline\ x\ DAMGO}$; $z$ = -2.436, $p < 0.05$. **(**I) Example traces for summary data shown in (H). * $p \leq 0.05$; ** $p \leq 0.01$; *** $p \leq 0.001$. Mean ± standard error of the mean. N: number of animals; n: number of recorded cells; Str: striatum; PL: prelimbic cortex.

**Figure 1 – figure supplement 2**

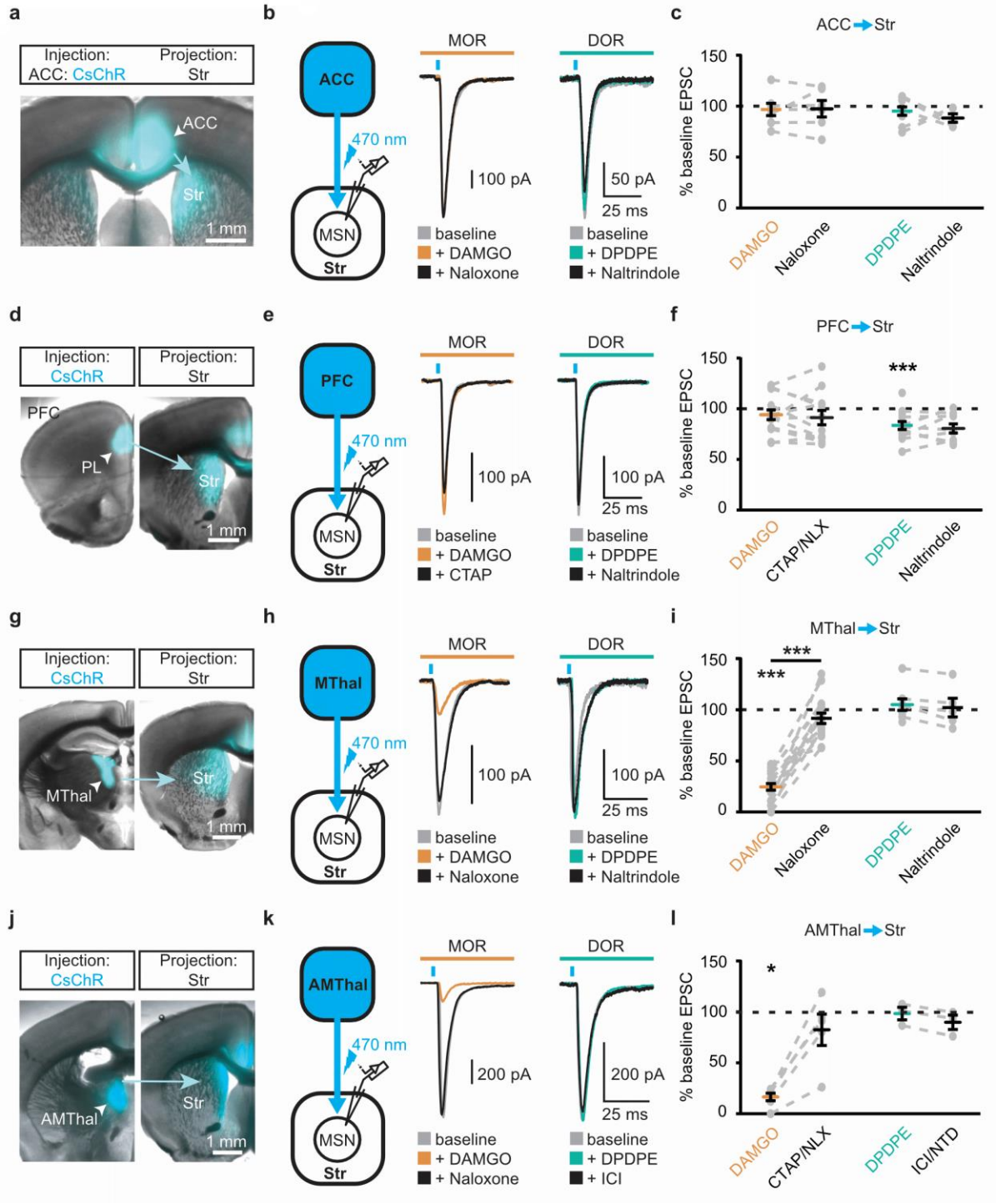


**Single channelrhodopsin injections reproduced specific effect of mu-opioid-mediated inhibition of thalamic but not cortical inputs.**

Virus expressing CsChR was injected into the ACC (A-C), the PFC (D-F), the MThal (G-I), or the anteromedial thalamus (AMThal) (J-L) as four sets of the experiments. (A, D, G, J) Representative images of the injection and projection for the above four sets of experiments, respectively. (B, E, H, K) Viral infection and optical stimulation schematic and example recordings of four sets of experiments, respectively. oEPSCs were evoked under baseline conditions (gray) and in the presence of DAMGO (1 µM, orange) followed by CTAP or naloxone (NLX) (1 µM, black), or DPDPE (1 µM, teal) followed by naltrindole (NTD) or ICI 174,864 (ICI) (0.3 µM, black). (C, F, I, L) Summary data of effects of DAMGO, CTAP/NLX, DPDPE, and ICI/NTD on oEPSC amplitude for the above four sets of experiments, respectively. (C) DAMGO/naloxone: N = 4/4, n = 7/6, *SM* = 0.054, p = 0.974; DPDPE/naltrindole: N = 5/4, n = 9/5, *SM* = 4.539, p = 0.103. (F) DAMGO/naloxone: N = 9/8, n = 14/12, *SM* = 2.286, p = 0.319. DPDPE/naltrindole: N = 9/6, n = 14/10, *SM* = 8.227, $p < 0.05$, $I_{DPDPE}$: 83.4 ± 3.9% of baseline, W (13) = 4, $p < 0.01$. (I) DAMGO/naloxone: N = 15/13, n = 19/16, *SM* = 25.660, $p < 0.001$, $I_{DAMGO}$: 24.5 ± 3.3% of baseline, W (19) = 0, $p < 0.001$, DAMGO vs. naloxone, W (12) = 0, $p < 0.001$; DPDPE/naltrindole: N = 7/5, n = 8/5, *SM* = 2.522, p = 0.283. (L) DAMGO/naloxone: N = 5/4, n = 6/5, *SM* = 9.399, $p < 0.01$, $I_{DAMGO}$: 16.5 ± 3.7% of baseline, W (6) = 0, $p < 0.05$; DPDPE/naltrindole: N = 2/2, n = 3/3, *SM* = 4.667, p = 0.097. Skillings-Mack test followed by paired Wilcoxon signed-ranks test *post-hoc* analysis. * $p \leq 0.05$; ** $p \leq 0.01$; *** $p \leq 0.001$. Mean ± standard error of the mean. *SM*: Skillings-Mack statistic.

**Figure 3 – figure supplement 1**

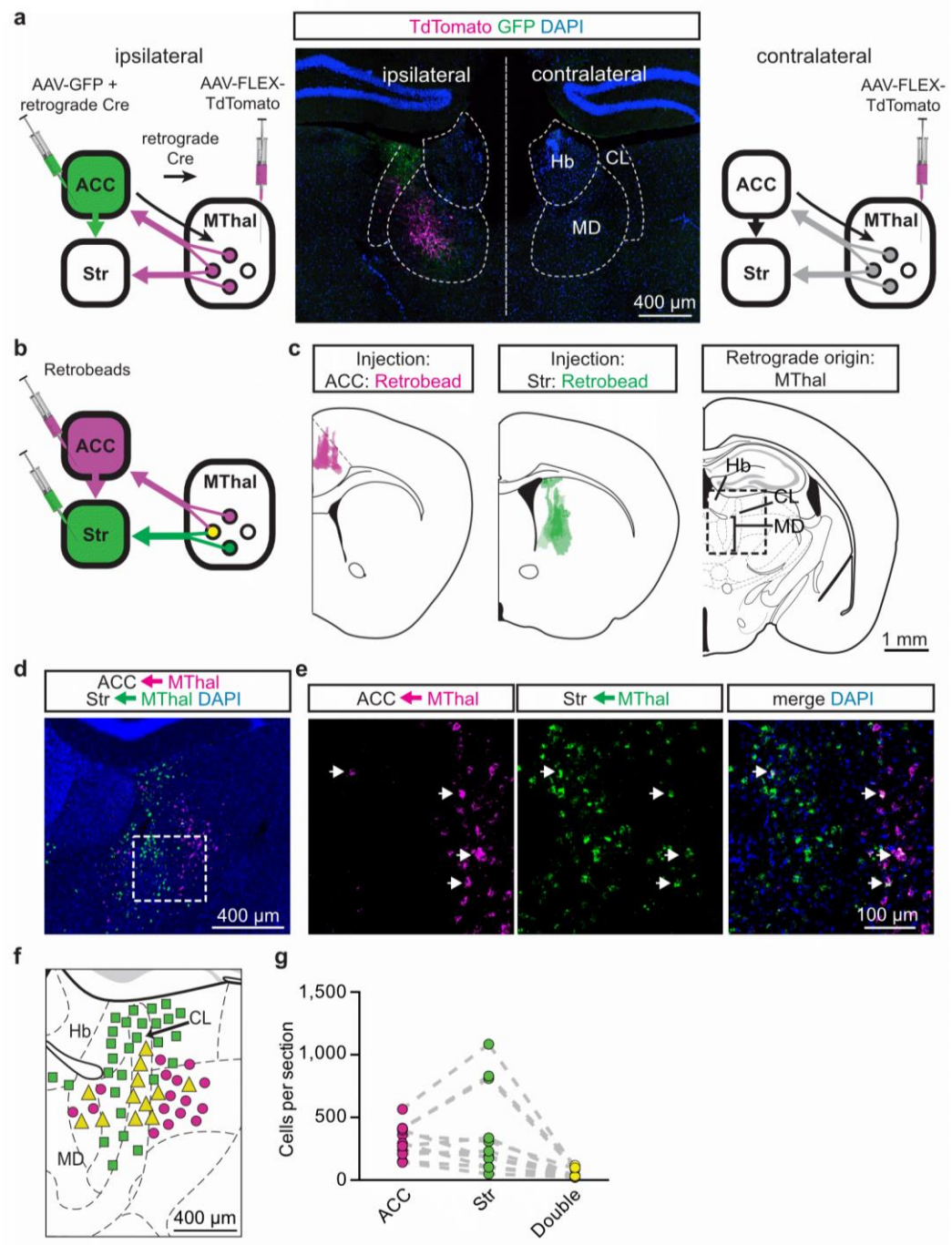


**A subset of mediodorsal thalamic neurons send collaterals to both the ACC and DMS.**

**(**A) Experimental diagram in which AAV2-FLEX-TdTomato was injected bilaterally into the MThal (left and right panels) and an example image of the labeling (middle panel). A

combination of AAV-GFP and AAV2-retro-Cre (retrograde Cre) was injected into the ACC (ipsilateral, left panel). DAPI-stained (blue) coronal brain slice with retrograde labeled thalamic neurons expressing TdTomato (red, amplified with anti-DsRed primary and Alexa 594 secondary antibodies) and GFP-positive axons (green, amplified with anti-GFP primary and Alexa 488 secondary antibodies) originating from the ACC (middle panel). (B) Experimental diagram of fluorescent retrograde bead injections into the ACC and the striatum. (C) Averaged retrobead injection sites are shown in relationship to the mouse brain atlas (left panel, magenta, and center panel, green) as described in (B). The region of interest in which fluorescent retrobeads were imaged and counted in the MThal is shown as the squared box on an atlas section (right panel). (D) Example image of retrobeads in the Mthal in ACC- (magenta) and Str-projecting (green) neurons from the area outlined in (C). € High magnification images of retrobeads in the MThal from the box outlined in (D). Arrowheads: neurons doubled labeled with both retrobeads (green and magenta). (F) Locations of retrograde labeled neurons surrounding the MThal were mapped onto the mouse brain atlas with estimation. Magenta circles: striatum-projecting neurons; green squares: ACC-projecting neurons; yellow triangles: striatum-projecting and ACC-projecting neurons. Note that the size of the markers is not to scale. (G) Summary graph showing the number of ACC (magenta), Str (green), or double labeled (yellow) retrobead clusters quantified per slice. Hb: habenula; CL: central lateral thalamus; MD: mediodorsal thalamus.

**Figure 4 – figure supplement 1**

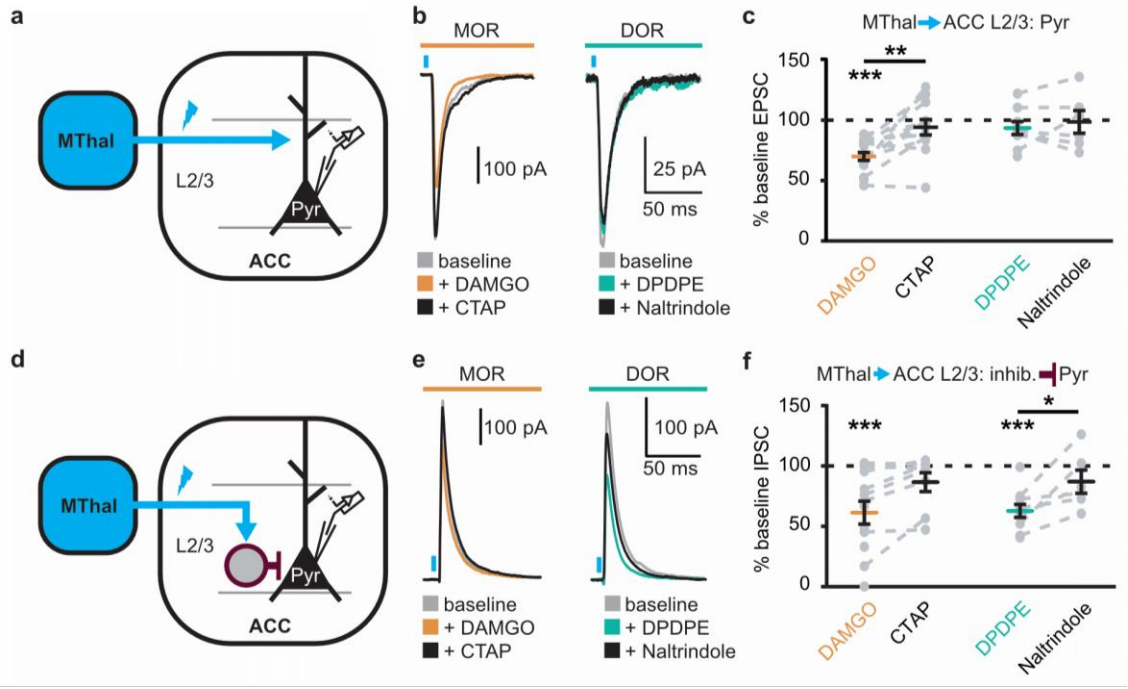


**Opioid inhibition of synaptic currents onto layer 2/3 pyramidal neurons in the ACC.**

(A) Experimental diagram in which ChR2(H134R) (blue) was injected in the MThal, and oEPSCs were recorded from Layer 2/3 (L2/3) pyramidal neurons (Pyr) in the ACC. (B) Example recordings of oEPSCs elicited from MThal terminals in the ACC. oEPSC amplitudes in response to DAMGO (1 µM, orange) followed by CTAP (1 µM, black) (left panel), and oEPSC amplitudes in response to DPDPE (1 µM, teal) followed by naltrindole (0.3 µM, black) (right panel). (C) Summary data of oEPSC amplitudes as described in (B), plotted as a percent of baseline. DAMGO: N = 8, n = 15; CTAP: N = 8, n = 12, *SM* = 18.148, $p < 0.001$, $I_{DAMGO}$: 69.3 ± 3.3% of baseline, $W(15) = 0$, $p < 0.001$; DAMGO vs. CTAP, $W(12) = 5$, $p < 0.01$; DPDPE: N = 7, n = 9; naltrindole: N = 6, n = 6, *SM* = 1.866, $p = 0.393$. (D) Experimental diagram in which ChR2(H134R) (blue) was injected in the MThal, and oIPSCs were recorded from L2/3 pyramidal neurons in the ACC. (E) Example recordings of oIPSCs elicited from MThal terminals in the ACC under baseline conditions, in response to DAMGO and CTAP, or DPDPE and naltrindole

as in (B). (F) Summary data of oIPSC amplitudes as described in (C, E), plotted as a percent of baseline. DAMGO: N = 7, n = 12; CTAP: N = 6, n = 8; *SM* = 8.882, $p < 0.05$, $I_{DAMGO}$: 61.2 ± 9.5% of baseline, W(12) = 1, $p < 0.001$; DPDPE: N = 7, n = 10; naltrindole: N = 5, n = 6, *SM* = 13.329, $p < 0.01$, $I_{DPDPE}$: 62.7 ± 5.4% of baseline, W(10) = 0, $p < 0.01$, DAMGO vs. CTAP, W(6) = 0, $p < 0.05$. Skillings-Mack test followed by paired Wilcoxon signed-rank test *post-hoc* analysis. * $p \leq 0.05$; ** $p \leq 0.01$; *** $p \leq 0.001$. Mean ± standard error of the Mean. inhib.: inhibitory neuron; *SM*: Skillings-Mack statistic.

**Figure 4 – figure supplement 2**

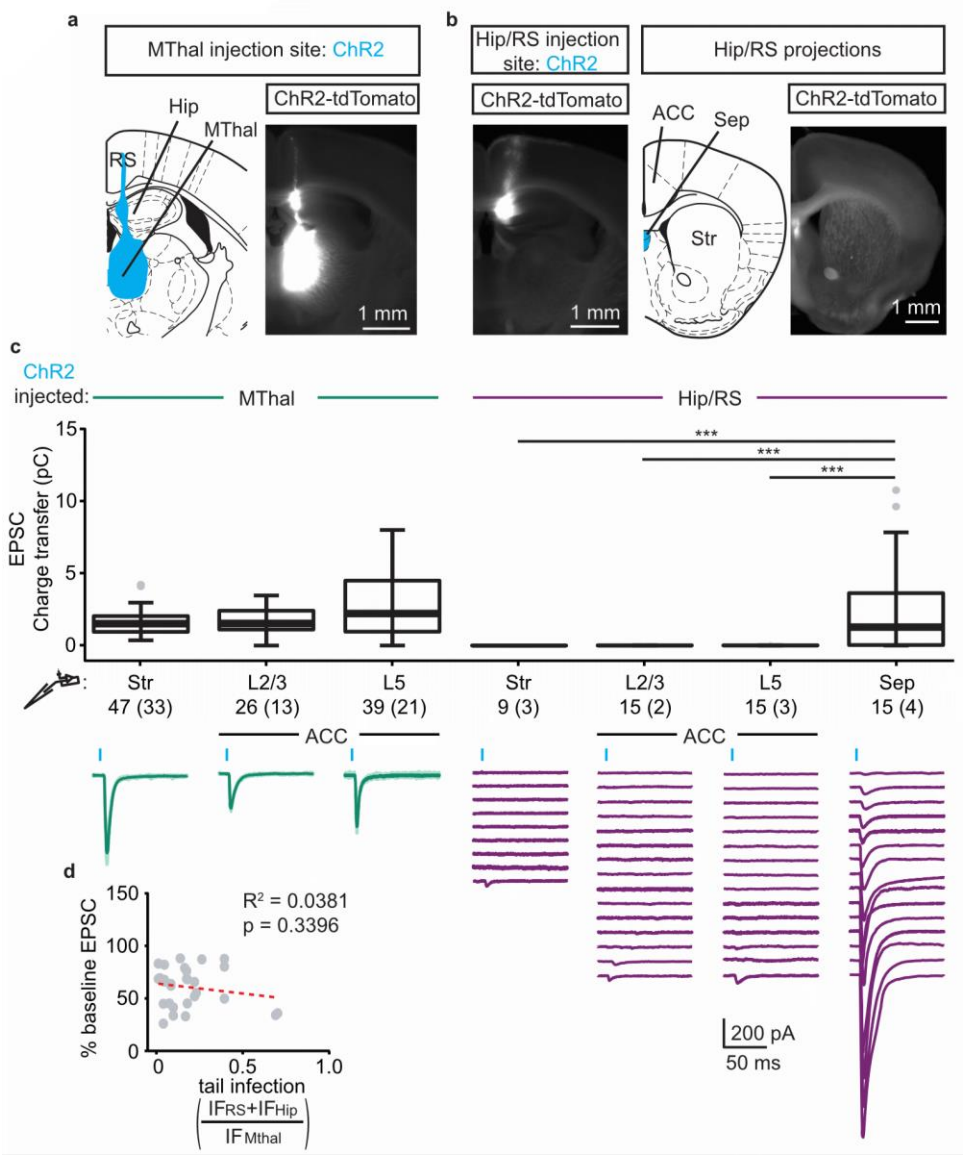


**Verification of origins of optically-evoked response.**

(A) Representative fluorescent image (right panel) of a typical MThal ChR2 injection in which virus was injected in the MThal while also infecting a "tail" region including hippocampus (Hip) and retrosplenial cortex (RS). The fluorescence at the injection site is saturated to reveal the "tail" region. Schematic of ChR2(H134R)-TdTomato expression shown in blue on a section of the atlas (left). (B) Example fluorescent image of ChR2(H134R)-TdTomato expressed only in

the "tail" region and corresponding image of projection areas (right) that highlight projections in the septum (Sep) but lack of visible projections in the ACC and striatum following Hip/RS "tail" injection. (C) Charge transfer of EPSCs (upper panel) recorded in striatal MSNs (Str), layer 2 and 3 (L2/3) or layer 5 (L5) pyramidal neurons following optical stimulation in mice injected with ChR2 in either MThal or Hip/RS, as well as Sep as a positive control for the Hip/RS injections. Hip/RS "tail" injections resulted in only occasional small amplitude oEPSCs in the Str and ACC. Kruskal-Wallis test, $H = 69.654$, $df = 6$, $p < 0.001$; post-hoc Dunn's test, Bonferonni-corrected. *** $p \leq 0.001$. Mean ± standard error of the mean. Representative average recordings (lower panel, dark green, average of 10 single trials) from the MSNs, L2/3 and L5 neurons upon optical stimulation of ChR2(H134R) injected in the MThal as shown in (A). Averaged oEPSCs (lower panel, purple, average of 10 single trials) of all individual neurons recorded in Hip/RS injected mice, as shown in (B). Blue bars: 470 nm light stimulations. (D) Plot of the DAMGO effect on baseline oEPSC amplitudes recorded in all L2/3 and L5 pyramidal neurons, as a function of the ratio of integrated fluorescence intensity (IF) of ChR2(H134R)-TdTomato fluorescence in RS + Hip ($IF_{RS}$ + $IF_{Hip}$) relative to MThal ($IF_{MThal}$) in all the Mthal injected groups. There was no correlation between the amount of "tail" infection and the degree of oEPSC inhibition by DAMGO. Linear regression model, $R^2 = 0.034$, $F(1, 27) = 0.945$, $p = 0.340$.

**Figure 6 – figure supplement 1**

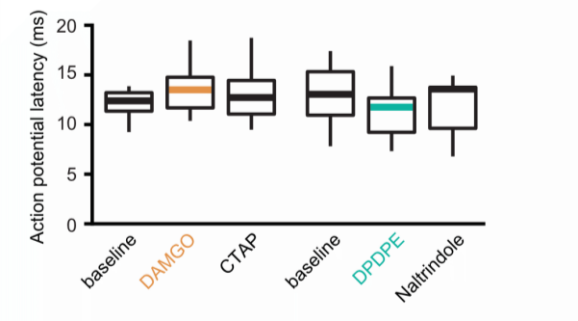


**Latencies of thalamocortical-evoked action potentials in ACC pyramidal neurons**.

The average latency to the first action potential following optical stimulation of the MThal inputs recorded in layer 5 (L5) pyramidal neurons (Pyr), using loose cell-attached configuration. There were no significant differences in the latency to the first spike. DAMGO: N = 3, n = 7; CTAP: N = 3, n = 7, *SM* = 2, p = 0.368; DPDPE: N = 4, n = 8; naltrindole: N = 4, n = 8, *SM* = 1.75, p = 0.417. *SM*: Skillings-Mack statistic.

**Figure 7 – figure supplement 1**

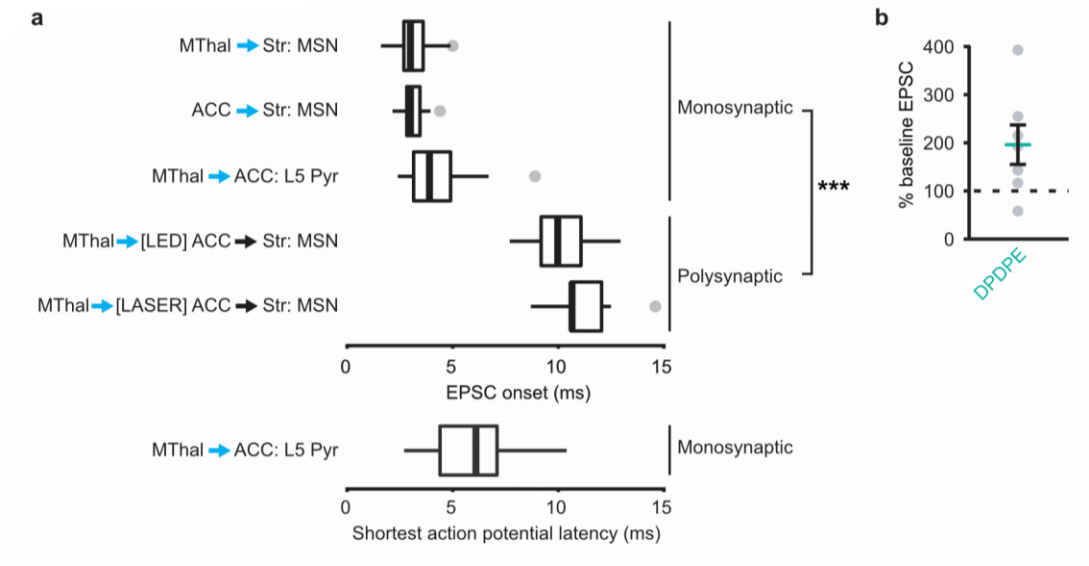


**EPSCs and action potential latencies within the thalamo-cortico-striatal circuits.**

(A) Average onset time for monosynaptic and polysynaptic EPSCs using either full field (LED stimulation: all monosynaptic data, and [LED] ACC polysynaptic data), or focal (laser stimulation: [LASER] ACC polysynaptic data) optical stimulation. Mann-whitney U test, U = 15, $p < 0.001$. *** $p \leq 0.001$. Box plot with median, 1st and 3rd quartile and whiskers represent 1.5 times interquartile range. Lower panel: average of shortest action potential onset latency in L5 pyramidal neurons following stimulation of MThal terminals. Stimulation intensity was set to elicit ~50% spike probability out of 50 trials. (B) EPSC amplitudes measured in MSNs in the striatum (Str) evoked by optical stimulation of MThal terminals in the ACC in the presence of DPDPE, plotted as a percentage of baseline EPSC. N = 6, n = 7, W (7) = 3, p = 0.078. Mean ± standard error of the mean.